Title:

Müller glia cell cycle re-activation by simultaneous cyclin D1 overexpression and p27^{kip1} knockdown promotes retinal regeneration in mice

Authors:

Zhifei Wu[1*], Baoshan Liao[1*], Julia Ying[1], Jan Keung[1,2], Zongli Zheng[1,2], Virpi Ahola[2,3], Wenjun Xiong[1]

Institutions:

1. Department of Biomedical Sciences, City University of Hong Kong, Hong Kong, China.
2. Ming Wai Lau Centre for Reparative Medicine, Karolinska Institutet, Hong Kong, China.
3. Institute of Biomedicine, University of Eastern Finland, Kuopio, Finland

* These authors contribute equally

Corresponding author: Wenjun Xiong

Email: wenjun.xiong@cityu.edu.hk

Address: The Department of Biomedical Sciences,
City University of Hong Kong,
Kowloon,
Hong Kong, China

Conflict of interest

The authors declare that no conflict of interest exists.

Abstract

Harnessing the regenerative potential of endogenous stem cells to restore lost neurons is a promising strategy for treating neurodegenerative disorders. Müller glia (MG), the primary glial cell type in the retina, exhibit remarkable regenerative abilities in lower vertebrate species, such as zebrafish and amphibians, where injury induces MG to proliferate and differentiate into various retinal neuron types. The regenerative potential of mammalian MG is constrained by their inherent inability to re-enter the cell cycle, likely due to high levels of the cell cycle inhibitor $p27^{Kip1}$ and low levels of cyclin D1 observed in adult mouse MG. In this study, we found that adeno-associated virus (AAV)-mediated cyclin D1 overexpression and $p27^{Kip1}$ knockdown exerts a strong synergistic effect on MG proliferation. MG proliferation induced by this treatment was potent but self-limiting, as MG did not undergo uncontrolled proliferation or lead to retinal neoplasia. Single-cell RNA sequencing (scRNA-seq) revealed that cell cycle reactivation leads to immunosuppression and dedifferentiation of MG. Notably, scRNA-seq analysis identified a new cluster of rod-like MG cells expressing both rod and MG genes, which was further validated by RNA in situ hybridization. Cell cycle reactivation also led to de novo genesis of bipolar- and amacrine-like cells from MG. Overall, our findings suggest that AAV-mediated cyclin D1 overexpression and $p27^{Kip1}$ knockdown stimulate MG proliferation and promote MG reprogramming. This approach may be a promising strategy, especially when combined with other regeneration-promoting factors, to enhance MG-mediated retinal repair.

Introduction

Müller glia (MG) is the last cell type generated by the retinal progenitor cells (RPCs) during development and exhibit a gene expression profile similar to that of late retinal progenitor cells (Jadhav et al., 2009; Roesch et al., 2012). In teleost fish and amphibians, MG respond rapidly to retinal injury, undergoing robust proliferation and regenerating lost retinal neurons from MG-derived progenitor cells (Hamon et al., 2016; Todd and Reh, 2022). In contrast, the proliferative and neurogenic ability of MG in response to injury in mammals is severely limited, failing to mediate retinal self-repair (Karl et al., 2008). Recent investigations have achieved great success in mammalian retinal regeneration by direct conversion of MG to retinal neurons through a single or combination of neurogenic transcription factors (Jorstad et al., 2017; Levi et al., 2021; Todd et al., 2022; Yumi et al., 2015). However, this may lead to a depletion of the MG population and cause further retinal degeneration, as MG are indispensable for retinal function and homeostasis. Other studies have shown that the quiescent state of MG can be overridden by upstream signaling pathways such as Wnt and Hippo (Hamon et al., 2019; Rueda et al., 2019; Yao et al., 2016). Activation of Wnt signaling by forced expression of β-catenin in adult mouse MG promoted spontaneous cell cycle re-entry in uninjured retinas (Yao et al., 2016). Moreover, it was demonstrated that bypassing the Hippo pathway in mouse MG led to spontaneous re-entry into the cell cycle and reprogramming into a progenitor cell-like state (Hamon et al., 2019; Rueda et al., 2019). These findings suggest that the re-entry of MG into the cell cycle, which is the first step of MG-mediated retinal regeneration in zebrafish, could be unlocked in mammalian retinas.

The cell cycle of MG is mainly regulated by cyclins and cyclin-dependent kinases (CDKs). Cyclins bind to CDKs to form cyclin-CDK complexes to promote cell cycle progression. During retinal development, the expression of D-type cyclins (cyclin D1, D2, and D3) is tightly regulated (Barton and Levine, 2008; Dyer and Cepko, 2001; Trimarchi et al., 2008). Among

68 these, cyclin D1, encoded by the *Ccnd1* gene, is the predominant D-type cyclin in the
69 developing retina and is highly expressed in the RPCs but absent in differentiated cells (Barton
70 and Levine, 2008; Trimarchi et al., 2008). Mice lacking *Ccnd1* have small eyes and
71 hypocellular retinas due to reduced RPC proliferation (Fantl et al., 1995; Sicinski et al., 1995),
72 which cannot be compensated by *Ccnd2* and *Ccnd3* (Das et al., 2012, 2009). Negative
73 regulators of the cell cycle are CDK inhibitors (CDKIs), which include the INK4 ($p16^{INK4a}$,
74 $p15^{INK4b}$, $p18^{INK4c}$, and $p19^{INK4d}$) and CIP/KIP families ($p21^{Cip1}$, $p27^{Kip1}$, and $p57^{Kip2}$)
75 (Reynisdóttir et al., 1995). The CDKIs inhibit cell cycle progression by binding to and
76 inactivating the cyclin-CDK complexes (Besson et al., 2008), and they regulate the
77 proliferation in distinct retinal progenitor cells (Dyer and Cepko, 2000a, 2001; Levine et al.,
78 2000). $p27^{Kip1}$ inhibits the cyclin D-CDK complex to enter of the S phase. Following acute
79 retinal damage in mice, a very small number of MG re-enter the cell cycle, co-incident with
80 the downregulation of $p27^{Kip1}$ or upregulation of cyclin D1 (Dyer and Cepko, 2000b; Hamon
81 et al., 2019; Rueda et al., 2019; Yao et al., 2016). However, this process is transient, as cyclin
82 D1 expression rapidly returns to the basal level (Dyer and Cepko, 2000; Hamon *et al.*, 2019a;
83 Rueda *et al.*, 2019).

84 In this study, we propose that targeting the two key regulators of the cell cycle, cyclin D1
85 and $p27^{kip1}$, can effectively induce MG cell cycle re-entry. Our findings demonstrate that
86 simultaneously reducing $p27^{Kip1}$ and increasing cyclin D1 in the MG using a single AAV vector
87 has a strong synergistic effect on promoting MG proliferation in uninjured adult mouse retinas.
88 MG proliferation induced by this treatment is robust and self-limiting, as MG undergo a single
89 round of cell division rather than unlimited proliferations. Through single-cell RNA
90 sequencing (scRNA-seq), we observed that cell cycle reactivation leads to immunosuppression
91 and dedifferentiation of the MG. Interestingly, scRNA-seq analysis also showed that a new
92 cluster of rod-like MG cells that express both rod and MG genes was induced by the treatment.

93 RNA in situ analysis further confirmed that MG cells in the outer nuclear layer (ONL) express
94 high levels of rod gene *Rho* and *Gnat1* while maintaining the expression of MG gene *Glul*.
95 Additionally, a few EdU+ MG daughter cells in the inner nuclear layer (INL) express the
96 bipolar cell marker Otx2 or the amacrine cell marker HuC/D, suggesting de novo neurogenesis
97 from MG. These results indicate that cell cycle reactivation also promotes MG reprogramming.
98 Importantly, MG cell cycle reactivation does not disrupt retinal structure or impair retinal
99 function, as the treatment did not deplete the MG from the retina. In summary, our results
100 showed that MG cell cycle reactivation by downregulating $p27^{Kip1}$ and upregulating cyclin D1
101 stimulates MG proliferation and promotes cell fate reprogramming, and it is possible to
102 combine this approach with other factors that promote regeneration in order to enhance retinal
103 repair mediated by MG.

Results

Simultaneous p27^{Kip1} downregulation and cyclin D1 overexpression drive robust MG proliferation in the uninjured mouse retina

To test the hypothesis that adult mouse MG are kept in a quiescent state by high levels of p27^{Kip1} and low levels of cyclin D1, we examined whether spontaneous MG proliferation can be activated by directly changing the levels of these two downstream cell cycle regulators. In this study, we used adeno-associated virus (AAV) serotype 7m8 vector and a promoter sequence cloned from the human *glial fibrillary acidic protein* (*GFAP*) gene to drive MG-specific gene expression (Fig. 1A, Supplementary Fig. 1) (Lee et al., 2008). AAV$_{7m8}$ vectors were injected intravitreally into the eyes of C57BL/6 mice on postnatal day 6 (P6), when MG finish proliferation and start differentiation, and intraperitoneal injections of 5-ethynyl-2'-deoxyurdine (EdU) were given for five consecutive days to label the MG that had entered the S phase of the cell cycle (Fig. 1B). In the control retinas infected with AAV$_{7m8}$-GFAP-GFP-nontarget (NT) short hairpin RNA (shRNA) virus, all MG, which were identified by Sox9 expression aligning in the inner nuclear layer (INL), were negative of EdU labeling (Fig. 1C). When the retina was infected by AAV$_{7m8}$-GFAP-mCherry-p27^{Kip1} shRNA, which expresses a highly efficient p27^{Kip1} shRNA, a small number of MG cells re-entered the cell cycle (Fig. 1D, G, Supplementary Fig. 2); however, these proliferated MG accounted for less than 1% of the total MG population. Similarly, overexpressing cyclin D1 alone through AAV$_{7m8}$-GFAP-cyclin D1 infection stimulated a subset of MG cells to proliferate, resulting in a three-fold increase in the number of EdU+ MG cells compared to p27^{Kip1} knockdown (Fig. 1E, G, Supplementary Fig. 3). Finally, the AAV$_{7m8}$-GFAP-cyclin D1-p27^{Kip1} shRNA vector, which simultaneously overexpressed cyclin D1 and suppressed p27^{Kip1}, had the most significant impact on MG proliferation, with a five-fold increase in EdU+Sox9+ cells compared to cyclin D1 overexpression alone (Fig. 1F, G, whole retinal cross-section shown in Supplementary Fig.

129 4). These findings suggest that both low levels of p27Kip1 and high levels of cyclin D1 are
130 required for postmitotic MG to re-enter the cell cycle. Henceforth, we refer to this AAV vector
131 that enables robust MG proliferation through concurrent $p27^{Kip1}$ knockdown and cyclin D1
132 overexpression as the cell cycle activator (CCA).

133 A transgenic mouse line *Glast-Cre^{ERT2}; Sun1:GFP*, in which MG nuclei were labeled by
134 nuclear membrane-bound GFP (Supplementary Fig. 5), was used to quantify the percentage of
135 MG that re-entered the cell cycle. In the retinal area where virus infection rate was the highest,
136 approximately 45% of Sun1:GFP+ MG were EdU positive (Fig. 1H), and the total number of
137 MG increased by about 50% (Fig. 1I), indicating that nearly half of the MG cells re-entered the
138 cell cycle. Previous research has shown that the ability of retina regeneration by various stimuli
139 declines with the age of the mice (Löffler et al., 2015; Ueki et al., 2015). We compared the
140 efficiency of CCA in driving MG proliferation in young (P28) and aged (>8 months) mouse
141 retinas to that in P6 pups. Remarkably, MG proliferation induced by CCA remained robust in
142 young adult and aged mice, with more than 200 EdU+Sox9+ cells per section (Fig. 1J). These
143 findings suggest that CCA efficiently drives MG proliferation in both young and aged animals.

144 **MG proliferation driven by CCA is self-limiting**

145 Concerned that $p27^{Kip1}$ suppression and cyclin D1 overexpression may lead to uncontrolled
146 cell proliferation and retinal tumorigenesis, we analysed the proliferative capacity of MG
147 driven by CCA. Firstly, we examined the duration of MG proliferation after CCA treatment by
148 a time-course EdU incorporation assay. On various days after the CCA injection, EdU was
149 administrated to label the cells that were undergoing proliferation (Fig. 2A). The result revealed
150 that MG proliferation started as quickly as the third day after CCA injection, reached its peak
151 around the fifth day, followed by a gradual decrease (Fig. 2A). By two weeks post CCA
152 injection, only a few MG were observed to have re-entered the cell cycle. Two months post-
153 CCA injection, MG proliferation had mostly ceased (Fig. 2A). These findings suggest that MG

154 proliferation was largely completed within 2 weeks post-CCA treatment, probably due to the
155 dilution of AAV episomal genome copies in the dividing cells. In addition, an EdU/BrdU
156 double-labeling assay was performed to examine whether MG undergoes one or multiple cell
157 divisions after CCA treatment. A single injection of EdU was given at 7 days post CCA
158 treatment, followed by BrdU injection 24 hours later (Fig. 2B). Retinas were collected 2 days
159 after BrdU injection to evaluate if any MG continuously entered the S phase of the cell cycle.
160 While there were a number of EdU+ cells and BrdU+ cells, few cells were co-labeled with EdU
161 and BrdU (Fig. 2B,C), indicating that MG undergoes only one cell division subsequent to CCA
162 treatment.

163 Next, we examined the distribution of the proliferated MG in the retina over time. As the
164 labelling efficiencies of MG by Tamoxifen-induced reporter expression and by EdU varied
165 among experiments and individual animals, we used the percentages of EdU+GFP+ MG in
166 each retinal layer to assess the distribution of the proliferated MG. During retina development,
167 proliferating retinal progenitor cells migrate in an apical-basal manner, whereas post-mitotic
168 cells migrate basally to reach their final laminar position (Lee and Norden, 2013). The
169 proliferating MG undergo similar interkinetic migration towards the apical surface of the retina,
170 as majority of the EdU+GFP+ MG nuclei were observed in the ONL and OPL (~53% and
171 ~22%, respectively) at one week after CCA treatment, which is around the peak time of MG
172 proliferation (Fig. 2D,E). To further explore whether the ONL MG daughter cells eventually
173 return to the INL over an extended period, we examined the distribution of EdU+ MG cells at
174 three weeks and four months post-CCA treatment. We found that while the percentage of INL
175 EdU+ MG increased slightly over time, there was still about half of EdU+ MG remained in the
176 ONL and in the OPL (Fig. 2D,E). Across the three time points examined, the absence of
177 EdU+GFP+ MG in the IPL and GCL suggests that migration of MG daughter cells to the GCL
178 does not occur, at least without injury (Fig. 2D,E). These findings led us to investigate whether

179 the long-term localization of MG daughter cells in the ONL and OPL is associated with any
180 change in their cell fate.

181 **Cell cycle re-activation drives downregulation of IFN pathway and MG dedifferentiation**

182 To unbiasedly assess the cell fate of MG and their daughter cells, we performed single-cell
183 RNA-Seq (scRNA-Seq) analysis on the mouse retinas that received CCA treatment. AAV_{7m8}-
184 GFAP-cyclin D1- $p27^{Kip1}$ shRNA and AAV_{7m8}-GFAP-GFP-NT shRNA (9:1 mixed) were co-
185 injected to stimulate MG proliferation in 4-week-old *Glast-Cre^{ERT2};tdTomato* mice (Fig. 3A),
186 and 10% AAV_{7m8}-GFAP-GFP-LacZsh was added to serve as an indicator of infection success.
187 The control group was injected with AAV_{7m8}-GFAP-GFP-NT shRNA to account for any non-
188 specific effect caused by virus injection and/or shRNA expression. Three weeks after virus
189 injection, the retinas with successful viral transduction were collected, and tdTomato+ cells
190 were isolated by fluorescence-activated cell sorting (FACS), followed by scRNA-seq (Fig. 3A).
191 As previous studies demonstrated that N-methyl-D-aspartate (NMDA)-induced retinal damage
192 and histone deacetylase inhibitor Trichostatin A (TSA) improve MG proliferation and
193 reprogramming (Hoang et al., 2020; Jorstad et al., 2017; Rueda et al., 2019) , a group of CCA-
194 treated mice also received NMDA on day 7 and TSA on day 9 post-CCA injection
195 (CCA+NMDA+TSA, referred to as CCANT) to enhance the reprogramming effect, if any, of
196 CCA.

197 After quality control, 3,758 cells were profiled in the control group, 3,890 cells in the CCA
198 group, and 3,278 cells in the CCANT group (Supplementary Figures 6 and 7). Clustering
199 analysis separated the cells into six different clusters (Fig. 3B), which are quiescent MG,
200 reactivated MG, MG in G2/M phase, MG in S phase, rod-like MG, and rods, as annotated by
201 the known retinal cell type markers (Fig. 3C). In the control group, the vast majority of MG
202 (>90%) remained as quiescent MG which express high levels of MG genes such as *Glul* and
203 *Kcnj10* (Fig. 3C-H). Cell cycle state analysis showed that a small percentage of cells are in the

204 G2/M or S phase in the CCA group, suggesting that there was still a small number of
205 proliferating MG at three weeks after CCA treatment (Fig. 3H, Supplementary Figure 7D,E).
206 In the CCA group, the majority of MG (~70%) formed a separate cluster, which we refer to as
207 reactivated MG. In this cluster of cells, we observed downregulation of MG genes (such as
208 *Glul* and *Kcnj10*) and upregulation of reactive gliosis gene *Gfap* and cell cycle inhibitor *Btg2*
209 compared with the quiescent MG cluster (Fig. 3H). Interestingly, the top differentially
210 expressed genes (DEGs) between reactivated MG and quiescent MG are the interferon (IFN)
211 pathway genes, including *Stat1*, *Stat2*, *Irgp1*, *Irgm1* and *Igtp*, which were downregulated in the
212 reactivated MG (Fig. 2F-H, Supplementary Fig. 8), while *Stat3* was not downregulated
213 concurrently with *Stat1* and *Stat2* (Supplementary Fig. 8). Here, downregulation of the IFN
214 pathway in the reactivated MG may be a direct response to cyclin D1 overexpression and/or
215 $p27^{Kip1}$ knockdown. A small percentage of MG (~8%) of reactivated MG was also present in
216 the control virus-injected group, which may be due to retinal injury caused by virus injection
217 and inflammatory response caused by the AAV virus (Fig. 3D, E). The cell clusters of the
218 CCANT group largely overlapped with the CCA group, with CCANT having fewer
219 proliferating cells and more reactivated MG.

220 **CCA upregulates rod gene expression in a subset of MG**

221 Interestingly, the rods and rod-like MG were two unexpected clusters that appeared in the
222 scRNA-seq analysis. Upon close examination of the retina of *Glast-Cre^{ERT2}; R26-tdTomato*
223 mice without Tamoxifen induction, we found that very few rods (14 Tdt+ rods in 128 whole
224 retinal sections of eight mouse retina samples screened) were mislabelled by leaky Tdtomato
225 expression in a Cre-independent manner (Supplementary Figure 9). The small rod clusters are
226 likely the true rods mislabelled by Tdt, which is presented in all three groups with a similar
227 proportion. The rod-like MG cluster resides between the reactivated MG cluster and the rod
228 cluster, and it is significantly enriched in the CCA and CCANT groups. The rod-like MG

229 expressed most rod genes, including *Rho*, *Gnat1, Rcvrn, Crx, and Nrl* (Fig. 3G, H,
230 Supplementary Fig. 10), although the expression levels of the rod-specific genes were lower
231 than those of natural rods. However, not all the rod genes are evenly upregulated, as the
232 upregulation of transcription factor *Otx2* that is crucial for rod cell fate specification and the
233 genes related to neuron projection and photoreceptor cell cilium such as *Syt1* and *Cacnb2* were
234 less significant (Supplementary Figure 10). In addition, the rod-like cells expressed a high level
235 of MG genes, while natural rods did not (Fig. 3G, H). When comparing the rod-like MG cluster
236 with the reactivated MG cluster, gene ontology (GO) analysis showed significant gene
237 enrichment in the pathways related to visual system development, neuron differentiation, visual
238 perception, and neuron projection (Supplementary Fig. 10). And GO was significantly enriched
239 in the genes associated with neuron projection and neuron differentiation in the rod cluster as
240 compared to the rod-like cluster (Supplementary Fig. 10), suggesting that rod-like MG were
241 not fully differentiated rods. When comparing the CCA- and CCANT-treated groups, NMDA
242 and TSA increased the percentages of reactivated MG and rod-like MG, but they did not induce
243 the fully differentiated rods or any other new cell clusters. In the following study, we focused
244 solely on the CCA treatment.

245 **Rod-like MG in the ONL expresses both rod and MG genes**

246 To exclude the possibility that the rod-like MG are fused MG with rod cell debris during retina
247 isolation for scRNA-seq analysis, we examined the expression of rod gene expression in the
248 rod-like MG on the retinal sections of the CCA-treated *Glast-Cre^{ERT2};Sun1:GFP* mice. As the
249 immunoreactivity for rod proteins such as RHO and GNAT1 is present in rod outer segment
250 (ROS), which are densely packed and distal from rod nuclei, we performed RNA in situ
251 hybridization on retinal sections using the RNAscope assay, which allowed us to analyse target
252 RNA abundance in rod nuclei with the preservation of the spatial information. We examined
253 the mRNA levels of the *Rho* and *Gnat1* genes at three weeks post CCA treatment, which is the

254 same harvest time point as in the scRNA-seq data. The signals of both probes are specific as
255 they are only detected in the ONL layer (Fig. 4A,B). In the control retinas, the mRNA of the
256 two rod genes was abundantly present in the rods in the ONL (Fig. 4A,C), while there was
257 minimal *Gnat1* and *Rho* mRNA in the MG in the INL (Fig. 4A,E). In the CCA-treated retina,
258 the MG in the ONL showed clear signals of both *Gnat1* and *Rho* mRNA (Fig. 4B,D), while the
259 INL MG maintained very low levels of *Gnat1* and *Rho* mRNA (Fig. 4B,F). We counted the
260 number of *Gnat1* fluorescent dots, which served as a reliable indicator of *Gnat1* mRNA levels.
261 The result showed a significant upregulation of *Gnat1* mRNA levels in the MG-derived cells
262 in the ONL and that its level was comparable to the natural rods (Fig.4G). The MG in the OPL
263 had intermediate levels of *Gnat1* mRNA, while the MG in the INL is similar to the untreated
264 MG controls (Fig. 4G). The *Rho* mRNA levels were quantified by measuring the pixel intensity
265 due to the fusion of numerous *Rho* fluorescent dots, which showed a similar trend of *Rho*
266 mRNA expression as that of *Gnat1* (Fig. 4H). The RNAscope result demonstrated that the MG-
267 derived cells in the ONL express high level of rod genes, those in the OPL express intermediate
268 level of rod genes, while all MG in the INL retained the no/low rod gene expression, suggesting
269 that the expression level of rod genes in the MG daughter cells is associated their position
270 within the retinal layers.

271 We further examined the expression level of the MG marker gene *Glul,* which encodes
272 Glutamate synthetase, in the MG cells located in different retinal layers (Fig. 5A-D). After
273 CCA treatment, the INL MG continue to express *Glul*, although the level is decreased (Fig.
274 5E), which is consistent with the downregulation of MG gene in the majority of the MG by
275 scRNA-seq. The MG-derived cells in the ONL expressed lower level of *Glul*, suggesting that
276 they retain the MG identity as well. The RNAscope results align with the scRNA-seq analysis,
277 indicating that the MG-derived cells in the ONL express both rod and MG genes at three weeks
278 post CCA treatment.

279 To find out whether the ONL MG could differentiate into mature rods if given an extended
280 period of time, we examined the morphology of the EdU+ MG in the ONL. Despite the
281 extensive search, we did not identify any EdU+ Tdt+ cells in the ONL with a ROS, which is
282 an important functional structure for rod phototransduction (Fig. 6A,B). Mature mouse rods
283 have a unique nuclear architecture, where heterochromatin localizes in a single large
284 chromocenter surrounded by euchromatin (Solovei et al., 2009). After CC treatment, the
285 majority of the ONL MG nuclei do not resemble the rod nuclei (Supplementary Figure 11A-
286 D). In addition, we labeled the MG sparsely with a low dose of Tamoxifen before CCA
287 treatment and found that most of the ONL MG daughter cells retained the apical processes
288 (Supplementary Figure 11E). We examined the mRNA expression of rod and MG genes again
289 at four months after CCA treatment. *Rho*, *Gnat1*, and *Glul* mRNA expression do not display
290 significant change at four months post-CCA treatment (Supplementary Fig. 12). Therefore, we
291 conclude that the ONL MG do not develop to mature rods despite the continuous expression
292 of rod gene and that they retained MG properties.

293 **Few bipolar and amacrine-like cells are regenerated from MG**

294 Bipolar (BP) and amacrine cells (AC) are two retinal neuron types that have been shown to be
295 regenerated from MG (Hoang et al., 2020; Jorstad et al., 2020, 2017). Although the scRNA-
296 seq data did not reveal other retinal neuron-like clusters derived from MG after CCA treatment,
297 we performed immunostaining of the bipolar marker Otx2 or the ganglion/amacrine maker
298 HuC/D to examine whether there are rare MG-derived cells expressing either marker. In order
299 to specifically identify *de novo* neurogenesis from MG and to exclude any mislabelled neurons
300 in the reporter mouse line, we focused our analysis on the EdU+Tdt+ MG in the *Glast-Cre*^{ERT2}*;*
301 *R26-tdTomato* mice. At four months post-CCA treatment, we observed less than 1% of the
302 total EdU+ Tdt+ cells expressing Otx2, whereas these cells were not present at three weeks
303 post-CCA treatment (Fig. 7A-E). We also found rare HuC/D+EdU+Tdt+ cells in the lower INL

304 where the HuC/D+ amacrine cells naturally reside (Fig. 7F-J). Whether these cells express
305 other BP or AC markers and whether they are functional interneurons that connect with the
306 retinal circuitry needs further investigation. Nonetheless, our findings suggest that cell cycle
307 re-activation alone can increase the plasticity of MG daughter cell fate, which allows some of
308 them to become BP or AC-like neurons.

309 **CCA does not cause retinal neoplasia or functional deficit**

310 To assess the long-term effect of CCA treatment, a cohort of C57BL/6 mice were observed for
311 a year following CCA injection (Fig. 7). Visual function assessments showed no significant
312 differences in visual acuity and electroretinography (ERG) between CCA-treated eyes and
313 uninjected control eyes one year after CCA treatment (Fig. 7A-C). Upon examining all the
314 harvested retinas from the CCA-treated group, no retinal neoplasia was observed. The retinal
315 structure remained intact, with no malignancy or disruptions in the retinal layers or
316 stratification (Fig. 7D,G). These results indicate that CCA treatment did not have a detrimental
317 impact on retinal structure or function in mice, nor did it induce retinal tumours.

318 We used the MG marker Sox9 to examine the MG population in the retina sections
319 harvested at a year post CCA treatment. In the control retina, Sox9+ MG cells were aligned in
320 the INL (Fig. 7D-E). In the CCA-treated retinas, there was a significant expansion in the
321 number of Sox9+ MG cells, distributed across the ONL, OPL, and INL (Fig. 7F-G). The large
322 population of Sox9+ MG remained to support the retinal homeostasis, which explains the
323 relatively unaffected retinal structure and function observed on the CCA-treated eyes. We
324 further made comparison of the numbers of Sox9+ cells after one year of CCA treatment and
325 after 2 weeks of CCA treatment. The total numbers of Sox+ cells were similar between these
326 two time points (Fig. 7H), indicating no significant MG loss after MG proliferation. To directly
327 assess whether CCA treatment may lead to the cell death of the MG, especially the MG
328 displaced in the ONL and OPL, we examined the CCA-treated retinas with TUNEL assay and

329 did not observe many TUNEL+ cells (Supplement Figure 13). Since we could only examine
330 cell death at single time points, we cannot completely exclude the possibility that there were
331 small numbers of MG-derived cells ding without being detected. The fact that the numbers of
332 MG in the ONL and OPL did not decrease in the retinas harvested at one-year post-CCA
333 treatment suggests that these MG-derived cells persist without dying or losing the MG identity
334 (Fig. 7I).

335 **Discussion**

336 MG proliferation is a key step towards MG-mediated regeneration in the retina. Previously, it
337 was shown that activation of the canonical Wnt pathway by AAV-mediated overexpression of
338 β-catenin stimulates MG proliferation through the Lin28/let7 pathway (Yao et al., 2016), and
339 cyclin D1 is a direct target gene of both Wnt signaling and Lin28/let7 (Li et al., 2012; Shtutman
340 et al., 1999; Tetsu and McCormick, 1999). Suppression of the Hippo pathway by transgenic
341 expression of *YAP5SA* induces MG proliferation, accompanied by an increase in cyclin D1
342 expression (Hamon et al., 2019; Rueda et al., 2019). However, the Hippo and Wnt pathways
343 have downstream genes besides cyclin D1 and serve different cellular functions. It is not clear
344 whether cyclin D1 activation is necessary or sufficient to drive MG proliferation in these
345 contexts. In this study, we demonstrated that cyclin D1 overexpression alone can promote MG
346 proliferation and that the combination of cyclin D1 overexpression and $p27^{Kip1}$ KD is the most
347 potent to drive MG proliferation in mouse retina without injury stimulus.

348 The strategy to stimulate the MG cell cycle for the purpose of retinal regeneration must be
349 carefully weighed against the concern of potential tumorigenesis. $p27^{Kip1}$ and cyclin D1 are
350 gatekeepers of cell cycle regulation, and any abnormalities in their expression may impact cell
351 division, potentially leading to the development of tumours. Previous studies have provided
352 evidence that mice lacking $p27^{Kip1}$ are approximately 30% larger and generally do not exhibit
353 malignancies, except for pituitary tumours that develop spontaneously (Fero et al., 1996).
354 Cyclin D1 is frequently overexpressed in a significant fraction of human cancers, such as breast
355 and respiratory tract tumours (Callender et al., 1994; Zukerberg et al., 1995). The concern
356 regarding retinal tumour formation due to CCA treatment may be mitigated, as the in vivo gene
357 transfer was performed using AAV vectors. The advantage of using AAV vector is that AAV
358 episomal genome becomes diluted after cell division, reducing the risk of tumor formation due
359 to continuous cyclin D1 overexpression and $p27^{Kip1}$ KD. Consistent with this, the rate of MG

360 proliferation was observed to decrease gradually over time, and the majority of MG cells did
361 not undergo multiple cell divisions (Fig. 2). Additionally, the retinal structure was normal
362 without neoplasia (Fig. 6,7). These results suggest that CCA is a potent and viable treatment
363 to stimulate MG proliferation and may be a promising approach to be used in combination with
364 other neurogenic factors to promote MG-mediated retinal regeneration.

365 Interestingly, we found that the IFN pathway genes are enriched in the top downregulated
366 genes in the reactivated MG cluster. The IFN pathway, mediated by STAT1 and STAT2, is an
367 important component of the innate immune system against viral infection and is also known as
368 antitumor cytokine signaling which facilitates immunosurveillance in tumor cells (Durbin et
369 al., 1996; Kaplan et al., 1998). This pathway has also been implicated in suppressing
370 regeneration in mice (Jorstad et al., 2020; Todd et al., 2020). STAT activation was shown to
371 reduce the ASCL1-induced retinal regeneration (Jorstad et al., 2020), and decreased IFN
372 signaling could be induced by microglia depletion, which improves MG neurogenic capacity
373 (Todd et al., 2020). In this study, we showed that the IFN pathway genes were downregulated
374 in the MG after CCA treatment. This would be a direct response to the upregulation of cyclin
375 D1 and/or downregulation of $p27^{kip1}$ in the MG cell-autonomously, or it could indirectly result
376 from the microglial responses elicited by the treatment. Investigating whether and how the
377 downregulation of IFN signaling plays a role in CCA-induced retinal regeneration would be
378 interesting questions to explore further.

379 The upregulation of rod genes in the MG residing in the ONL is an unexpected outcome of
380 MG cell cycle activation by CCA, as this was not reported in the other studies focusing on MG
381 proliferation (Hamon et al., 2019; Rueda et al., 2019; Yao et al., 2016). In those studies, a very
382 small subset of proliferative MG differentiated into BP and/or AC-like, but no photoreceptor
383 genesis was reported. In our study, a significant subset of MG expressed the mRNA of *Rho*
384 and *Gnat1* by scRNA-seq and RNAscope. However, the rod-like MG is unlikely a result of

385 MG-to-rod cell fate reprogramming, as we did not see many cells overexpressing neurogenic
386 genes, such as *Ascl1* and *Dll3*, or rod precursor gene *prdm1* (Supplementary Figure 14A).
387 scRNA-seq analysis at earlier time points after CCA treatment would be helpful to further
388 exclude this possibility. How does CCA activate rod gene expression if it is not through cell
389 fate reprogramming? One hypothesis is that cyclin D1 or $p27^{kip1}$ regulates rod gene expression
390 in addition to their well-characterized functions in cell cycle regulation. It was shown that
391 cyclin D1 possesses transcriptional functions by recruiting CREB-binding protein histone
392 acetyltransferase in developing mouse retinas (Bienvenu et al., 2010). Cyclin D has been shown
393 to activate retinoblastoma protein (Rb) by mono-phosphorylation (Narasimha *et al.*, 2014), and
394 Rb in turn promotes rod maturation, which is independent of its function for RPC cell cycle
395 exit (Zhang *et al.*, 2004). In the $Rb1^{-/-}$ retinal explants, many genes expressed in rods, such as
396 Nrl and Nr2e3, were significantly downregulated (Zhang *et al.*, 2004). Additionally, $p27^{xic1}$,
397 the Xenopus homolog of mammalian $p27^{kip1}$, has been shown to promote glial cell fate
398 independent of its CDK binding activity (Ohnuma et al., 1999). Therefore, besides cell cycle
399 activation, cyclin D1 overexpression and/or $p27^{kip1}$ KD may promote rod gene expression
400 directly or indirectly, which may explain the rod-like MG population observed following CCA
401 treatment.

402 Although rod-like MG express rod genes, they are, by no means, mature rods. First of all,
403 they lack ROS and nuclear architecture of the mature rods. In addition, their gene expression
404 profile was different from that of natural rod. We compared gene expression profiles of rod-
405 like cells with natural rods and found that rod-like cells still lacked the expression of some
406 genes related to neuron projection and photoreceptor cell cilium such as *Syt1* and *Cacnb2*
407 (Supplementary Figure 10), indicating that rod-like cells were not fully differentiated. In
408 addition, the rod-like MG still expressed MG genes such as *Glul*. By comparing differentially
409 expressed genes associated with cell differentiation, we found that Notch-related genes,

410 including *Notch1* and its downstream gene *Hes1*, remain highly expressed in the reactivated
411 and rod-like MG (Supplementary Figure 14B). Notch signaling pathway is involved in
412 regulating both cell proliferation and cell fate specification during retinal development (Jadhav,
413 Mason and Cepko, 2006; Yaron *et al.*, 2006). Genetic removal of *Notch1*, or Notch downstream
414 effectors such as *Hes1* and *RBP*-J leads to precocious cell cycle exit and increased
415 photoreceptors production during early retinogenesis (Tomita et al., 1996; Jadhav, Mason and
416 Cepko, 2006; Riesenberg et al., 2009; Zheng et al., 2009). In addition, Notch1 functions in
417 postmitotic cell fates to repress the rod fate (Mizeracka, Demaso and Cepko, 2013). Therefore,
418 we conjecture that the high activity of Notch signaling may be the reason why rod-like cells
419 fail to become full differentiated rods. A recent preprint has shown that suppressing Notch
420 signaling in the MG and deletion of nuclear factor I factors a, b, and x (Nfia/b/x) synergize to
421 promote neurogenesis of MG into retinal bipolar and amacrine interneurons in adult mice after
422 NMDA-induced retinal injury (Le et al., 2023).
423

424 **Limitations of the study:**

425 One unresolved question is how to further enhance rod regeneration by combining CCA with
426 other factors. It remains to be tested whether inhibiting Notch signaling or overexpressing other
427 neurogenic factors, in combination with CCA treatment, can result in the full differentiation of
428 new rod photoreceptors. Additionally, while the CCA approach exhibited potent mitogenic
429 activity in uninjured mouse retinas, its ability to promote MG proliferation after retinal injury
430 is still unknown. Further investigation is needed to test the effects of CCA in mouse models of
431 retinal degeneration. Finally, it is yet to be investigated how the CCA treatment affects the
432 promoter accessibility of rod genes in the rod-like MG cells. Single-cell ATAC-seq or ChIP-
433 seq analyses could provide insights into the epigenetic changes that underlie the rod-like
434 phenotype acquired by the proliferated MG cells.

435 **Materials and Methods**

436 **Animals**

437 Wild-type mice (strain C57BL/6J), Rosa26-tdTomato reporter mice (strain *B6.Cg-*
438 *Gt(ROSA)26Sor*$^{tm14(CAG\text{-}tdTomato)Hze}$*/J*), *Rosa26-Sun1:GFP* reporter mice (Strain *B6.129-*
439 *Gt(ROSA)26Sor*$^{tm5.1(CAG\text{-}Sun1/sfGFP)Nat}$*/MmbeJ*), and *Glast-CreER* reporter mice (strain
440 *Tg(Slc1a3-cre/ERT)1Nat/J)* mice were purchased from the Jackson Laboratory and were kept
441 on a 12 hour light/12 hour dark cycle. All animal procedures performed were approved by the
442 Hong Kong Department of Health under Animals Ordinance Chapter 340, and animal care was
443 carried out in accordance with institutional guidelines.

444 **AAV plasmids and vectors**

445 pAAV-GFAP-GFP vector plasmid was cloned by replacing the CMV promoter with a 681bp
446 ABC_1D region of the human *GFAP* gene promoter (Lee et al., 2008) into the pAAV-CMV-
447 GFP vector (Supplementary Figure 1A). cDNAs encoding mouse cyclin D1 were cloned into
448 AAV plasmids by Gibson ligation. AAV-shRNA vectors were cloned by replacing the GFP
449 sequence with mCherry-shRNA in the pAAV-GFAP-GFP vector. pAAV-GFAP-cyclinD1-P27
450 shRNA and pAAV-GFAP-GFP-LacZ shRNA were cloned by replacing mCherry sequence
451 with cyclinD1 and GFP from the pAAV-GFAP-mCherry-P27 shRNA1 and pAAV-GFAP-
452 mCherry-LacZ shRNA, respectively (Supplementary Figure 2A). pAAV rep/Cap 2/2, and
453 Adenovirus helper plasmids were obtained from the University of Pennsylvania Vector Core,
454 Philadelphia. pAAV7m8 plasmid (#64839) was purchased from addgene.

455 AAV was produced in HEK293T cells (HCL4517; Thermo Scientific) by AAV vector, rep/cap
456 packaging plasmid, and adenoviral helper plasmid co-transfection followed by iodixanol
457 gradient ultracentrifugation. Purified AAVs were concentrated with Amicon 100K columns
458 (EMD Millipore) to a final titer higher than 5×10^{13} genome copies/mL. Protein gels were run
459 to determine virus titers.

460 **Tamoxifen injection**

461 Intraperitoneal injections of tamoxifen (Sigma) in corn oil were administered to induce the
462 expression of Cre recombinase. Starting from P20, tamoxifen was given at a dosage of 50
463 mg/kg daily for 5 consecutive days to label as many MG as possible. For the purpose of sparse
464 labeling, a single dose of tamoxifen at 15 mg/kg was administered on P20.

465 **AAV injection**

466 Intravitreal injection was performed using a pulled angled glass pipette controlled by a
467 FemtoJet (Eppendorf). The tip of the needle was passed through the sclera at the equator, near
468 the dorsal limbus of the eyeball, and entered into the vitreous cavity. The injection volume of
469 AAVs (5 x 10^{13} genome copies/mL) was 0.5μl per eye for P6 injection and 1μl per eye for adult
470 mouse injection.

471 ***In situ* RNA hybridization**

472 *In situ* RNA hybridization was performed using the RNAscope Multiplex Fluorescent
473 Detection Reagents V2 kit (Advanced Cell Diagnostics) following the commercial protocols.
474 In brief, retinas were dissected, 4% PFA fixed, dehydrated in sucrose solution and embedded
475 in optimal cutting temperature (OCT) medium. Retinas were cryosectioned into 20μm and
476 mounted on SuperFrost Plus glass slides (Epredia). After OCT removal by PBS and further
477 dehydration by ethanol, retinal sections were stained with GFP antibody (AB_2307313; Aves
478 Labs) at 4 °C overnight. After three times wash with PBST (PBS with 0.1% Tween-20), retinal
479 sections were hybridized with RNA probes (Advanced Cell Diagnostics Cat.No. 474801-C3
480 for Mm *Rho*, 524881-C2 for Mm *Gnat1*, 426231-C2 for Mm *Glul*) for 2 hours at 40 °C for two
481 hours. Following in situ RNA hybridization steps, slides were stained using secondary
482 antibodies (Jackson ImmunoResearch) and DAPI for two hours at room temperature. The
483 fluorescent signals were visualized and captured using Nikon A1HD25 High speed and Large
484 Field of View Confocal Microscope. The mRNA levels inside the GFP labelled nuclei

485 membrane were quantified as number of RNA dots or measured as signal intensity level by
486 ImageJ.

487 **Immunohistochemistry**

488 Retinas were dissected and fixed in 4% formaldehyde in PBS for 30 min at room temperature
489 and sectioned at 20-μm thickness by cryostat. Retinal sections were blocked in 5% BSA in
490 PBST (PBS with 0.1% Triton X-100), stained with primary antibodies at 4 °C overnight, and
491 washed three times with PBST. Primary antibodies used in this study included rabbit anti-
492 $p27^{kip1}$(1:200, PA5-16717; Thermofisher); rabbit anti-cyclin D1 antibody (1:300, 26939-1-AP;
493 Proteintech), goat anti-Otx2 antibody (1:200, AF 1979; R&D systems), mouse anti-HuC/D
494 antibody (1:200, A21271; Thermofisher), rabbit anti-GFAP antibody (Z0334, 1:500, DAKO),
495 rabbit anti-Sox2 antibody (1:2000, ab97959; abcam) and rabbit anti-Sox9 antibody (1:1000,
496 AB5535; Millipore). Sections were stained using secondary antibodies (Jackson
497 ImmunoResearch) for two hours at room temperature. Cell nuclei were counterstained with
498 DAPI (Sigma). TUNEL was performed using an TUNEL BrightRed Apoptosis Detection Kit
499 (Vazyme) according to the manufacturer's protocol.

500 **EdU incorporation and BrdU detection assay**

501 5'-ethynyl-2'-deoxyuridine (EdU, 50mg/kg, Abcam ab146186) or 5-bromo-2' deoxyuridine
502 (BrdU,100mg/kg, Abcam 142567) was intraperitoneally injected to label the cells in the S
503 phase. EdU staining was performed using the Click-iT™ EdU Alexa Fluor™ 488 Imaging Kit
504 (C10337). For BrdU detection, the retinal sections were incubated with 2 M HCl for 1 hour at
505 room temperature. The sections were rinsed with PBST and incubated with a blocking buffer
506 containing 5% BSA in PBST for 2 hours at room temperature. Primary antibody mouse anti-
507 BrdU (1:300, ab8152; Abcam) was stained overnight at 4 °C, and secondary antibodies
508 (Jackson ImmunoResearch) were stained for 2 hours at room temperature.

509 **Single-cell RNA-seq**

510 *Library preparation and sequencing of single cells*

511 The FACS-sorted cells from each sample were filtered through 40 µm strainer (pluriStrainer)
512 and processed with Chromium Next GEM Single Cell 3′ GEM, Library & Gel Bead Kit v3.1
513 (1000269), Chromium Next GEM Chip G Single Cell Kit (1000127) and Chromium Controller
514 (10x Genomics) according to the manufacturer's protocol. The constructed libraries were sent
515 to Novogene (Beijing) for NovaSeq paired-end 150 bp sequencing and produced 330 Gb of
516 raw data.

517 *Preprocessing, filtering and clustering of scRNA data*

518 Sequencing results were preprocessed with 10x Genomics Cell Ranger 6.1.1. (Zheng et al.,
519 2017) for demultiplexing, barcode assignment, and unique molecular identifier (UMI)
520 quantification using a standard pipeline for 10X for each of the three samples. We used indexed
521 mouse genome mm10 with added tdTomato and GFP transgenes as a reference. Reads mapping
522 to introns covered more than 34% of all reads. Therefore, they were included in feature counts
523 by using 'include_introns' option in cellranger count step of the pipeline. Cell Ranger
524 aggregation was applied for merging runs from three samples.

525 Quality control, filtering, dimensional reduction, and clustering of the data were carried out
526 using the Seurat package in R (Stuart et al., 2019). The cells with less than 2,000 expressed
527 features, total UMI count higher than 100,000 and percentage of mitochondrial transcripts more
528 than 15% were disregarded. Features of the Y chromosome, as well as *Xist* and *Tsix* genes of
529 the X chromosome, were excluded to avoid confusing effects of gender.

530 Further filtering of cells was carried out by only including cells expressing tdTomato
531 (Supplementary Figure 6). Potential cell duplicates were estimated using DoubletFinder
532 method (McGinnis et al., 2019) implemented in R (with parameter settings PC=10, pK=0.28,
533 pN=0.3). The threshold for the expected doublet formation rate was set to 10% to reflect the

534 assumption that cell duplicates can appear relatively commonly in the MG cells. Detected
535 duplicates were excluded from the data (Supplementary Figure 6G,H).
536 For the remaining cells, Uniform Manifold Approximation and Projection (UMAP) dimension
537 reduction based on eight principal components (PCs) was applied, and cells were clustered
538 using the graphical clustering method in Seurat. Cell types were identified using known marker
539 genes (Clark et al., 2019; Hoang et al., 2020). After removing doublets, cell types in clusters
540 4-9 other than MG, Rod-like, and Rod included only a few cells, and 10-30% of the cells were
541 from the control sample, suggesting that these cells are likely to be contaminated
542 (Supplementary Figure 6I,J). After excluding cells in clusters 4-9, the new UMAP and
543 clustering (Supplementary Figure 7A) revealed two subclusters of Rod-like cells (Clusters C3-
544 C4, Supplementary Figure 7A). The cells in the subcluster C4 exhibited similar proportional
545 contributions from all three groups and expressed lower level of rod-specific genes such as *Rho*
546 (Supplementary Figure 7B,C). These cells were again defined as contaminated and excluded
547 from the data. The final UMAP was constructed using seven PCs, and the same PCs were used
548 for clustering of cells (Figure 3B).
549 *Analysis of scRNA-seq data*
550 The cell cycle state of each cell was defined by the Cell Cycle Scoring function in the Seurat
551 R package. The cells with G2/M and S scores lower than 0.1 were defined to be proliferating
552 (Supplementary Figure 7D,E). Differential gene expression analysis between different cell
553 types or three treatment groups was performed using Deseq2 (Supplementary table 1) (Love et
554 al., 2014). Enrichment analysis of top 200 up- and downregulated genes was performed for
555 Gene Ontologies (GO), KEGG and Reactome pathways using Gprofiler2 R interface to
556 g:Profiler (Raudvere et al., 2019).
557 **The optomotor and electroretinography tests**

558 Mouse visual acuity was measured using an Optometry System (Cerebral Mechanics Inc.)
559 following the published protocol (Douglas et al., 2005). Testing was done with a grating of 12
560 degrees/second drifting speed and 100% contrast. The injected right eyes (CCA treated) and
561 uninjected left eyes (Ctrl) were tested independently for counterclockwise and clockwise
562 grating rotations, respectively. A staircase procedure was used, in which the observer tested
563 low to high visual acuity. Each animal was tested for about 10-15 minutes per session.

564 ERG was measured using an Espion E3 System (Diagonsys LLC Inc.) as previously described
565 (Hoang et al., 2023). Animals were dark-adapted overnight before the test. After inducing
566 anesthesia with a ketamine: xylazaine injection intraperitoneally, the pupils of both eyes were
567 dilated using Mydrin®-P Ophthalmic Solution. Once the pupils were fully dilated, the eyes
568 were maintained moist using a topical gel. The measurement electrodes were then applied to
569 the cornea of both eyes, while the ground electrodes were attached to the mouth and tail. All
570 these steps were performed in the darkroom under dim red light. For scotopic ERG recordings,
571 a multiple 530nm light with different intensities (increments from 0.01 cd.s/m^2 to 30 cd.s/m^2)
572 were elicited to stimulate scotopic responses in a specific time interval. For photopic ERG
573 recordings, 5 mins exposure under 10 cd.s/m^2 light intensity was adopted to inhibit the rod
574 function. The photopic response was measured by multiple flashes of 30 cd.s/m^2 intensity in
575 the illuminated background (10 cd.s/m^2). The average amplitude and implicit time of a- and b-
576 wave were recorded and exported for further analysis. The b-wave amplitude of the step-wise
577 scotopic responses and that of photopic response at 30 cd.s/m^2 were shown in figure.
578

579 **Statistics**

580 Data were represented as mean ± SEM in all figures. Sample sizes and statistical analysis were
581 indicated for each experiment in figure legend. ANOVA analysis with Tukey test was
582 performed to compare multiple groups, and Student's t-test to compare two groups. A P value

583 of $P < 0.05$ was considered statistically significant. GraphPad Prism was used to perform
584 statistical analysis and make figures.
585

586 **Acknowledgements:**
587 This research was funded by Research Grants Council Hong Kong Project (11103819,
588 11102922, and 11100723), Hong Kong Health and Medical Research Fund Project (05160276
589 and 06172466), TUNG Biomedical Sciences Foundation, and Ming Wai Lau Center for
590 Reparative Medicine Research Associate Program.

591 **References:**

592 Barton KM, Levine EM. 2008. Expression patterns and cell cycle profiles of PCNA, MCM6,
593 cyclin D1, cyclin A2, cyclin B1, and phosphorylated histone H3 in the developing mouse retina.
594 *Dev Dyn* **237**:672–682.

595 Besson A, Dowdy SF, Roberts JM. 2008. CDK inhibitors: cell cycle regulators and beyond.
596 *Dev Cell* **14**:159–169.

597 Bienvenu F, Jirawatnotai S, Elias JE, Meyer CA, Mizeracka K, Marson A, Frampton GM, Cole
598 MF, Odom DT, Odajima J, Geng Y, Zagozdzon A, Jecrois M, Young RA, Liu XS, Cepko CL,
599 Gygi SP, Sicinski P. 2010. Transcriptional role of cyclin D1 in development revealed by a
600 genetic-proteomic screen. *Nature* **463**:374–378.

601 Callender T, el-Naggar AK, Lee MS, Frankenthaler R, Luna MA, Batsakis JG. 1994. PRAD-1
602 (CCND1)/cyclin D1 oncogene amplification in primary head and neck squamous cell
603 carcinoma. *Cancer* **74**:152–158.

604 Clark BS, Stein-O'Brien GL, Shiau F, Cannon GH, Davis-Marcisak E, Sherman T, Santiago
605 CP, Hoang TV, Rajaii F, James-Esposito RE, Gronostajski RM, Fertig EJ, Goff LA, Blackshaw
606 S. 2019. Single-cell RNA-seq analysis of retinal development identifies NFI factors as
607 regulating mitotic exit and late-born cell specification. *Neuron* **102**:1111-1126.e5.

608 Das G, Choi Y, Sicinski P, Levine EM. 2009. Cyclin D1 fine-tunes the neurogenic output of
609 embryonic retinal progenitor cells. *Neural Dev* **4**:15.

610 Das G, Clark AM, Levine EM. 2012. Cyclin D1 inactivation extends proliferation and alters
611 histogenesis in the postnatal mouse retina. *Dev Dyn* **241**:941–952.

612 Douglas RM, Alam NM, Silver BD, McGill TJ, Tschetter WW, Prusky GT. 2005. Independent
613 visual threshold measurements in the two eyes of freely moving rats and mice using a virtual-
614 reality optokinetic system. *Vis Neurosci* **22**:677–684.

615 Durbin JE, Hackenmiller R, Simon MC, Levy DE. 1996. Targeted disruption of the mouse
616 Stat1 gene results in compromised innate immunity to viral disease. *Cell* **84**:443–450.
617 Dyer MA, Cepko CL. 2001. p27Kip1 and p57Kip2 regulate proliferation in distinct retinal
618 progenitor cell populations. *J Neurosci* **21**:4259–4271.
619 Dyer MA, Cepko CL. 2000a. p57(Kip2) regulates progenitor cell proliferation and amacrine
620 interneuron development in the mouse retina. *Development* **127**:3593–3605.
621 Dyer MA, Cepko CL. 2000b. Control of Müller glial cell proliferation and activation following
622 retinal injury. *Nat Neurosci* **3**:873–880.
623 Fantl V, Stamp G, Andrews A, Rosewell I, Dickson C. 1995. Mice lacking cyclin D1 are small
624 and show defects in eye and mammary gland development. *Genes Dev* **9**:2364–2372.
625 Fero ML, Rivkin M, Tasch M, Porter P, Carow CE, Firpo E, Polyak K, Tsai L-H, Broudy V,
626 Perlmutter RM, Kaushansky K, Roberts JM. 1996. A syndrome of multiorgan hyperplasia with
627 features of gigantism, tumorigenesis, and female sterility in p27 -deficient mice. *Cell* **85**:733–
628 744.
629 Hamon A, García-García D, Ail D, Bitard J, Chesneau A, Dalkara D, Locker M, Roger JE,
630 Perron M. 2019. Linking YAP to Müller Glia quiescence exit in the degenerative retina. *Cell*
631 *Rep* **27**:1712-1725.e6.
632 Hamon A, Roger JE, Yang X-J, Perron M. 2016. Müller glial cell-dependent regeneration of
633 the neural retina: An overview across vertebrate model systems. *Dev Dyn* **245**:727–738.
634 Hoang DA, Liao B, Zheng Z, Xiong W. 2023. Mutation-independent gene knock-in therapy
635 targeting 5'UTR for autosomal dominant retinitis pigmentosa. *Signal Transduct Target Ther*
636 **8**:100.
637 Hoang T, Wang J, Boyd P, Wang F, Santiago C, Jiang L, Yoo S, Lahne M, Todd LJ, Jia M,
638 Saez C, Keuthan C, Palazzo I, Squires N, Campbell WA, Rajaii F, Parayil T, Trinh V, Kim

639 DW, Wang G, Campbell LJ, Ash J, Fischer AJ, Hyde DR, Qian J, Blackshaw S. 2020. Gene
640 regulatory networks controlling vertebrate retinal regeneration. *Science* **370**:eabb8598.
641 Jadhav AP, Roesch K, Cepko CL. 2009. Development and neurogenic potential of Müller glial
642 cells in the vertebrate retina. *Prog Retin Eye Res* **28**:249–262.
643 Jorstad NL, Wilken MS, Grimes WN, Wohl SG, VandenBosch LS, Yoshimatsu T, Wong RO,
644 Rieke F, Reh TA. 2017. Stimulation of functional neuronal regeneration from Müller glia in
645 adult mice. *Nature* **548**:103–107.
646 Jorstad NL, Wilken MS, Todd L, Finkbeiner C, Nakamura P, Radulovich N, Hooper MJ,
647 Chitsazan A, Wilkerson BA, Rieke F, Reh TA. 2020. STAT signaling modifies Ascl1
648 chromatin binding and limits neural regeneration from Muller Glia in adult mouse retina. *Cell*
649 *Rep* **30**:2195-2208.e5.
650 Kaplan DH, Shankaran V, Dighe AS, Stockert E, Aguet M, Old LJ, Schreiber RD. 1998.
651 Demonstration of an interferon γ-dependent tumor surveillance system in immunocompetent
652 mice. *Proc Natl Acad Sci U S A* **95**:7556–7561.
653 Karl MO, Hayes S, Nelson BR, Tan K, Buckingham B, Reh TA. 2008. Stimulation of neural
654 regeneration in the mouse retina. *Proc Natl Acad Sci U S A* **105**:19508–19513.
655 Le N, Vu T-D, Palazzo I, Pulya R, Kim Y, Blackshaw S, Hoang T. 2023. Robust
656 reprogramming of glia into neurons by inhibition of Notch signaling and NFI factors in adult
657 mammalian retina. *bioRxivorg*. doi:10.1101/2023.10.29.560483
658 Lee HO, Norden C. 2013. Mechanisms controlling arrangements and movements of nuclei in
659 pseudostratified epithelia. *Trends Cell Biol* **23**:141–150.
660 Lee Y, Messing A, Su M, Brenner M. 2008. GFAP promoter elements required for region-
661 specific and astrocyte-specific expression. *Glia* **56**:481–493.

662 Levi MJ, Hooper AK, Haugan C, Finkbeiner N, Jorstad N, Radulovich CK. 2021. Efficient
663 Stimulation of Retinal Regeneration from Müller Glia in Adult Mice Using Combinations of
664 Proneural bHLH Transcription Factors.
665 Levine EM, Close J, Fero M, Ostrovsky A, Reh TA. 2000. p27(Kip1) regulates cell cycle
666 withdrawal of late multipotent progenitor cells in the mammalian retina. *Dev Biol* **219**:299–
667 314.
668 Li N, Zhong X, Lin X, Guo J, Zou L, Tanyi JL, Shao Z, Liang S, Wang L-P, Hwang W-T,
669 Katsaros D, Montone K, Zhao X, Zhang L. 2012. Lin-28 homologue A (LIN28A) promotes
670 cell cycle progression via regulation of cyclin-dependent kinase 2 (CDK2), cyclin D1
671 (CCND1), and cell division cycle 25 homolog A (CDC25A) expression in cancer. *J Biol Chem*
672 **287**:17386–17397.
673 Löffler K, Schäfer P, Völkner M, Holdt T, Karl MO. 2015. Age-dependent Müller glia
674 neurogenic competence in the mouse retina. *Glia* **63**:1809–1824.
675 Love MI, Huber W, Anders S. 2014. Moderated estimation of fold change and dispersion for
676 RNA-seq data with DESeq2. *Genome Biol* **15**:550.
677 McGinnis CS, Murrow LM, Gartner ZJ. 2019. DoubletFinder: Doublet detection in single-cell
678 RNA sequencing data using artificial nearest neighbors. *Cell Syst* **8**:329-337.e4.
679 Ohnuma S, Philpott A, Wang K, Holt CE, Harris WA. 1999. p27Xic1, a Cdk inhibitor,
680 promotes the determination of glial cells in Xenopus retina. *Cell* **99**:499–510.
681 Raudvere U, Kolberg L, Kuzmin I, Arak T, Adler P, Peterson H, Vilo J. 2019. g:Profiler: a web
682 server for functional enrichment analysis and conversions of gene lists (2019 update). *Nucleic*
683 *Acids Res* **47**:W191–W198.
684 Reynisdóttir I, Polyak K, Iavarone A, Massagué J. 1995. Kip/Cip and Ink4 Cdk inhibitors
685 cooperate to induce cell cycle arrest in response to TGF-beta. *Genes Dev* **9**:1831–1845.

686 Roesch K, Stadler MB, Cepko CL. 2012. Gene expression changes within Müller glial cells in
687 retinitis pigmentosa. *Mol Vis* **18**:1197–1214.
688 Rueda EM, Hall BM, Hill MC, Swinton PG, Tong X, Martin JF, Poché RA. 2019. The Hippo
689 pathway blocks mammalian retinal Müller glial cell reprogramming. *Cell Rep* **27**:1637-1649.e6.
690 Shtutman M, Zhurinsky J, Simcha I, Albanese C, D'Amico M, Pestell R, Ben-Ze'ev A. 1999.
691 The cyclin D1 gene is a target of the beta-catenin/LEF-1 pathway. *Proc Natl Acad Sci U S A*
692 **96**:5522–5527.
693 Sicinski P, Donaher JL, Parker SB, Li T, Fazeli A, Gardner H, Haslam SZ, Bronson RT,
694 Elledge SJ, Weinberg RA. 1995. Cyclin D1 provides a link between development and
695 oncogenesis in the retina and breast. *Cell* **82**:621–630.
696 Solovei I, Kreysing M, Lanctôt C, Kösem S, Peichl L, Cremer T, Guck J, Joffe B. 2009. Nuclear
697 architecture of rod photoreceptor cells adapts to vision in mammalian evolution. *Cell* **137**:356–
698 368.
699 Stuart T, Butler A, Hoffman P, Hafemeister C, Papalexi E, Mauck WM 3rd, Hao Y, Stoeckius
700 M, Smibert P, Satija R. 2019. Comprehensive integration of single-cell data. *Cell* **177**:1888-
701 1902.e21.
702 Tetsu O, McCormick F. 1999. Beta-catenin regulates expression of cyclin D1 in colon
703 carcinoma cells. *Nature* **398**:422–426.
704 Todd L, Finkbeiner C, Wong CK, Hooper MJ, Reh TA. 2020. Microglia suppress Ascl1-
705 induced retinal regeneration in mice. *Cell Rep* **33**:108507.
706 Todd L, Jenkins W, Finkbeiner C, Hooper MJ, Donaldson PC, Pavlou M, Wohlschlegel J,
707 Ingram N, Rieke F, Reh TA, Mu X. 2022. Reprogramming Müller glia to regenerate ganglion-
708 like cells in adult mouse retina with developmental transcription factors. *Sci Adv* **8**:eabq7219.
709 Todd L, Reh TA. 2022. Comparative biology of vertebrate retinal regeneration: Restoration of
710 vision through cellular reprogramming. *Cold Spring Harb Perspect Biol* **14**:a040816.

711 Trimarchi JM, Stadler MB, Cepko CL. 2008. Individual retinal progenitor cells display
712 extensive heterogeneity of gene expression. *PLoS One* **3**:e1588.
713 Ueki Y, Wilken MS, Cox KE, Chipman L, Jorstad N, Sternhagen K, Simic M, Ullom K,
714 Nakafuku M, Reh TA. 2015. Transgenic expression of the proneural transcription factor Ascl1
715 in Müller glia stimulates retinal regeneration in young mice. *Proc Natl Acad Sci U S A*
716 **112**:13717–13722.
717 Yao K, Qiu S, Tian L, Snider WD, Flannery JG, Schaffer DV, Chen B. 2016. Wnt regulates
718 proliferation and neurogenic potential of Müller glial cells via a Lin28/let-7 miRNA-dependent
719 pathway in adult mammalian retinas. *Cell Rep* **17**:165–178.
720 Yumi MS, Wilken KE, Cox L, Chipman N, Jorstad K, Sternhagen M, Simic K, Ullom M,
721 Nakafuku TA. 2015. Transgenic Expression of the Proneural Transcription Factor Ascl1 in
722 Müller Glia Stimulates Retinal Regeneration in Young Mice. *Proceedings of the National*
723 *Academy of Sciences of the United States of America* **112**:13717–13722.
724 Zheng GXY, Terry JM, Belgrader P, Ryvkin P, Bent ZW, Wilson R, Ziraldo SB, Wheeler TD,
725 McDermott GP, Zhu J, Gregory MT, Shuga J, Montesclaros L, Underwood JG, Masquelier
726 DA, Nishimura SY, Schnall-Levin M, Wyatt PW, Hindson CM, Bharadwaj R, Wong A, Ness
727 KD, Beppu LW, Deeg HJ, McFarland C, Loeb KR, Valente WJ, Ericson NG, Stevens EA,
728 Radich JP, Mikkelsen TS, Hindson BJ, Bielas JH. 2017. Massively parallel digital
729 transcriptional profiling of single cells. *Nat Commun* **8**:14049.
730 Zukerberg LR, Yang WI, Gadd M, Thor AD, Koerner FC, Schmidt EV, Arnold A. 1995. Cyclin
731 D1 (PRAD1) protein expression in breast cancer: approximately one-third of infiltrating
732 mammary carcinomas show overexpression of the cyclin D1 oncogene. *Mod Pathol* **8**:560–
733 567.

734 **Figure legends:**

735 **Figure 1. Simultaneous p27^{Kip1} downregulation and cyclin D1 overexpression drive robust MG**
736 **proliferation in the uninjured mouse retina**

737 (A) Schematic of AAV vectors used in this study. (B) Experimental design. (C-F) Analysis of EdU
738 incorporation. Uninjured mouse eyes were injected with (C) AAV-GFAP-mCherry-non target
739 (NT) shRNA (control), (D) AAV-GFAP-mCherry-p27 shRNA, (E) AAV-GFAP-cyclin D1,
740 and (F) AAV-GFAP-cyclin D1-p27 shRNA (CCA) at P6 and harvested at P18 after 5-day EdU
741 intraperitoneal injection. Retinal sections were co-labeled for MG marker Sox9. (G)
742 Quantification of EdU+ Sox9+ cells. AAV-GFAP-mCherry-NT shRNA control virus (n=8),
743 AAV-GFAP-mCherry-p27shRNA (n=11), AAV-GFAP-cyclin D1 (n=8), and CCA (n=14). (H)
744 Quantification of the percentages of EdU+GFP+ and EdU-GFP+ cells in the area with efficient
745 virus infection in the *Glast-CreERT2; Sun1:GFP* mouse retina injected with the control or
746 CCA vector. (I) Quantification of the total GFP+ MG in the *CreERT2; Sun1:GFP* retina
747 infected by CCA. Retinal area (250 μm in width) with the most efficient virus infection in the
748 middle retina region was selected for quantification. (J) Quantification of EdU+ Sox9+ cells in
749 the young (CCA injection at P6, n=13), adult (CCA injection at P28, n=17), and aged retinas
750 (CCA injection at P255-P347, n=7). ONL, outer nuclear layer; OPL, outer plexiform layer;
751 INL, inner nuclear layer; IPL, inner plexiform layer; GCL, ganglion cell layer. Data are
752 presented as mean ± SEM. * P<0.05; *** P<0.001; ns=not significant by one-way ANOVA
753 analysis with Tukey's post-hoc test (G, J) and two-tail unpaired student t-test (I).

754

755 **Figure 2. MG proliferation driven by CCA is self-limiting**

756 (A) Time-course analysis of MG proliferation after CCA injection. EdU was administered for
757 two consecutive days, starting from different days after the CCA injection, and samples were
758 harvested for analysis one day after the second EdU injection. Data are presented as mean ±

759 SEM, n≥4. (B) Analysis of EdU and BrdU labeled cells. (C) Quantification of the number of
760 EdU+BrdU-, EdU-BrdU+ and EdU+ BrdU+ cells. Data are presented as mean ± SEM. n≥4.
761 (D) Representative retinal sections of *Glast-CreERT2; Sun1:GFP* mice at one week, two weeks,
762 and four months post CCA injection. (E) Quantification of MG daughter cell (EdU+GFP+)
763 distribution in each retinal layer. ONL, outer nuclear layer; OPL, outer plexiform layer; INL,
764 inner nuclear layer; IPL, inner plexiform layer; GCL, ganglion cell layer. Data are presented
765 as mean ± SEM, n=3.
766
767 **Figure 3. scRNA-seq analysis of MG at three weeks post CCA treatment**
768 (A) Schematic illustration of scRNA-seq experiment. (B) UMAP plot of scRNA-seq data for
769 MG treated with CCA, CCANT, and control virus, with clusters identified by the known
770 marker gene expression. (C) Expression of retinal cell markers in different cell clusters. (D)
771 Split UMAP plots of the control, CCA, and CCANT groups. (E) The proportion of cell clusters
772 in the control, CCA, and CCANT groups. (F) Heatmap of top DEG genes between cell clusters.
773 Cells are shown in columns, and genes are in rows. Color scale denotes Z score of the
774 normalised gene expression levels. (G) The violin diagram shows the expression of IFN
775 pathway, MG and Rod genes in different cell clusters. (H) Feature plots of cell cycle regulator
776 (*Mik67*, *Mcm5*), glial (*Glul*, *Kcnj10*), gliosis (*Gfap*), cell proliferation (*Btg2*), and rod (*Rho* and
777 *Nrl*) normalised gene expression in different cell clusters. CCA, cell cycle activator; CCANT,
778 cell cycle activator + NMDA + TSA.
779
780 **Figure 4. *Gnat1* and *Rho* mRNA are expressed in the ONL and OPL MG**
781 (A-B) *Gnat1* and *Rho* mRNA in situ hybridization in the control (A) and the *Glast-*
782 *CreERT2;Sun1:GFP* mouse retinas harvested at three weeks post CCA injection (B). (C-F)
783 Magnified views of the highlighted regions in (A) and (B). (G) The number of *Gnat1* mRNA

784 dots per GFP+ cell and (H) the average pixel level of *Rho* mRNA per GFP+ cell. n=3 mice,
785 data are presented as mean ± SEM. ns=not significant, **P* < 0.05; ***P* < 0.01; ****P* < 0.001;
786 *****P* < 0.0001, by one-way ANOVA with Tukey's post hoc test (G, H).
787
788 **Figure 5. *Glul* mRNA level is decreased in the ONL and OPL MG**
789 (A-B) *Glul* mRNA in situ hybridization. (C-D) Magnified views of the highlighted regions in
790 (A) and (B). (E) The average pixel level of *Glul* mRNA per GFP+ cell. n=3 mice, data are
791 presented as mean ± SEM. ns=not significant, **P* < 0.05; ***P* < 0.01; ****P* < 0.001;
792 *****P* < 0.0001, by one-way ANOVA with Tukey's post hoc test (E).
793
794 **Figure 6. CCA induces de novo genesis of Otx2+ BP-like and HuC/D+ AC-like cells from**
795 **MG**
796 (A-B) Representative retinal sections of *Glast-CreERT2; tdTomato* mice at four months post
797 injection of CCA. Sections were immunostained with EdU and Otx2. (C-D) Magnified views
798 of the highlighted regions in (B). (E) Quantification of tdT+EdU+Otx2+/ tdT+EdU+%.
799 (F-G) Representative retinal sections immunostained with EdU and HuC/D. (H-I) Magnified
800 views of the highlighted regions in (F) and (G). (J) Quantification of
801 tdT+EdU+HuC/D+/tdT+EdU+%. n=3 mice, data are presented as mean ± SEM. *p<0.05;
802 **p<0.01, by unpaired two-tailed Student's t-test (E, J).
803
804 **Figure 7. CCA does not lead to retinal neoplastic transformation**
805 (A-C) Optomotor and electroretinography (ERG) tests were performed on wild type mice at 1
806 year after CCA injection (n≥4). Visual acuity by the optomotor test (A), and b-wave amplitudes
807 of the scotopic ERG under different light intensity in (B) and photopic ERG under 30 cd × s/m^2
808 in (C), respectively. Data are presented as mean ± SEM. ns=not significant by two-tail unpaired

809 Student's t-test (A-C). (D-E) Sox9 immunofluorescence in untreated control mice (D) and WT
810 mice one year after CCA injection (E). (F-G) Zoom-in images of the indicated area in (D) and
811 (E). (H) Quantification of the number of Sox9+ cells in retinas at two weeks or one year after
812 CCA injection and in age-corresponding WT control retinas. (I) Quantification of the number
813 of Sox9+ cells in each retinal layer. Data are presented as mean ± SEM. ns=not significant, **p
814 ≤0.01, ***p ≤0.001 by one-way ANOVA with Tukey's post hoc test (H) and two-tail unpaired
815 Student's t-test (I).

Figure 1

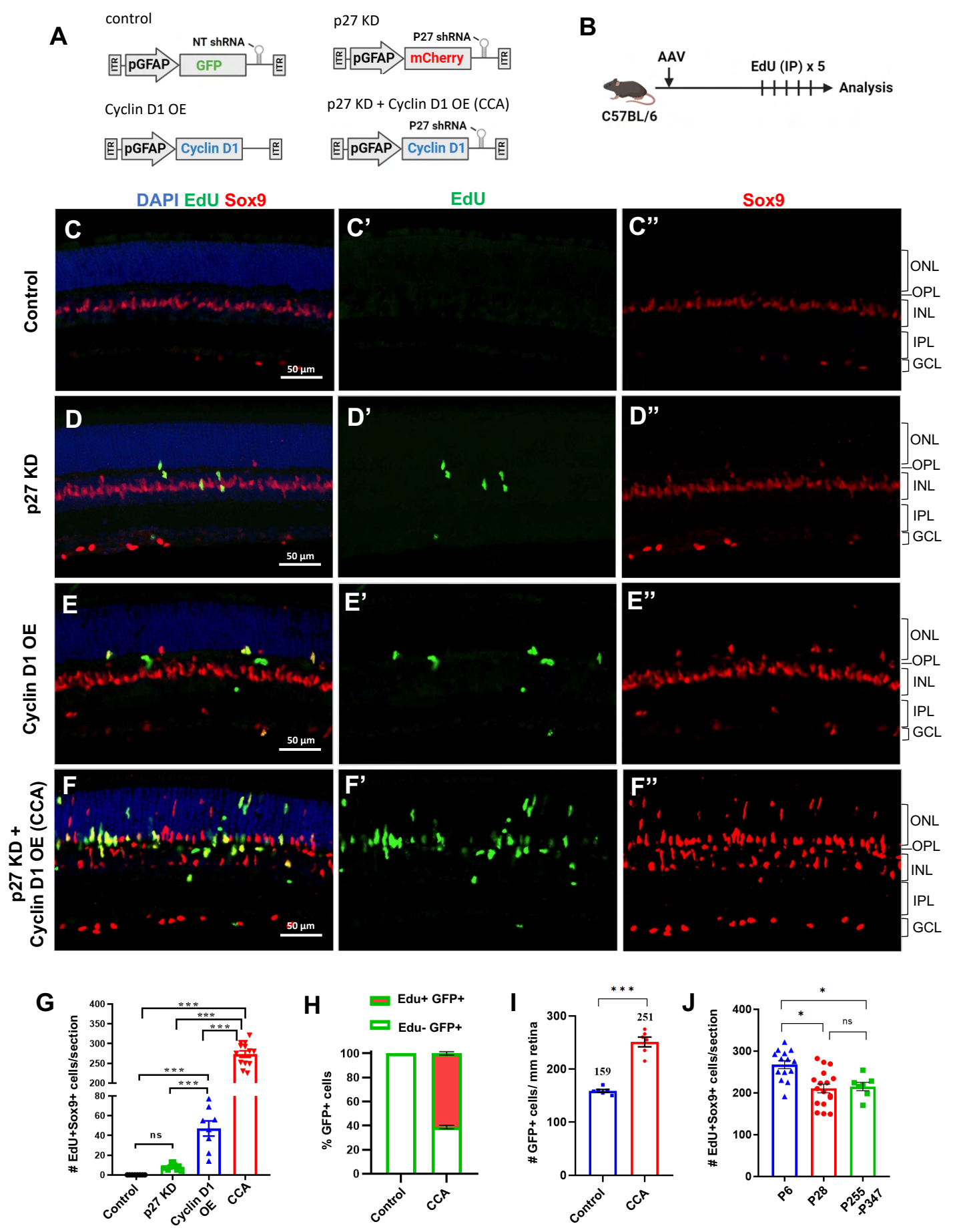
A
control
NT shRNA
ITR
pGFAP
GFP
ITR
p27 KD
P27 shRNA
pGFAP
mCherry
Cyclin D1 OE
pGFAP
Cyclin D1
p27 KD + Cyclin D1 OE (CCA)
P27 shRNA
pGFAP
Cyclin D1
B
AAV
EdU (IP) x 5
Analysis
C57BL/6
DAPI EdU Sox9
EdU
Sox9
Control
p27 KD
Cyclin D1 OE
p27 KD + Cyclin D1 OE (CCA)
C
C'
C''
D
D'
D''
E
E'
E''
F
F'
F''
50 µm
ONL
OPL
INL
IPL
GCL
G
EdU+Sox9+ cells/section
ns
Control
p27 KD
Cyclin D1 OE
CCA
H
Edu+ GFP+
Edu- GFP+
% GFP+ cells
Control
CCA
I
GFP+ cells/ mm retina
159
251
Control
CCA
J
EdU+Sox9+ cells/section
ns
P6
P28
P255 +P347

Figure 2

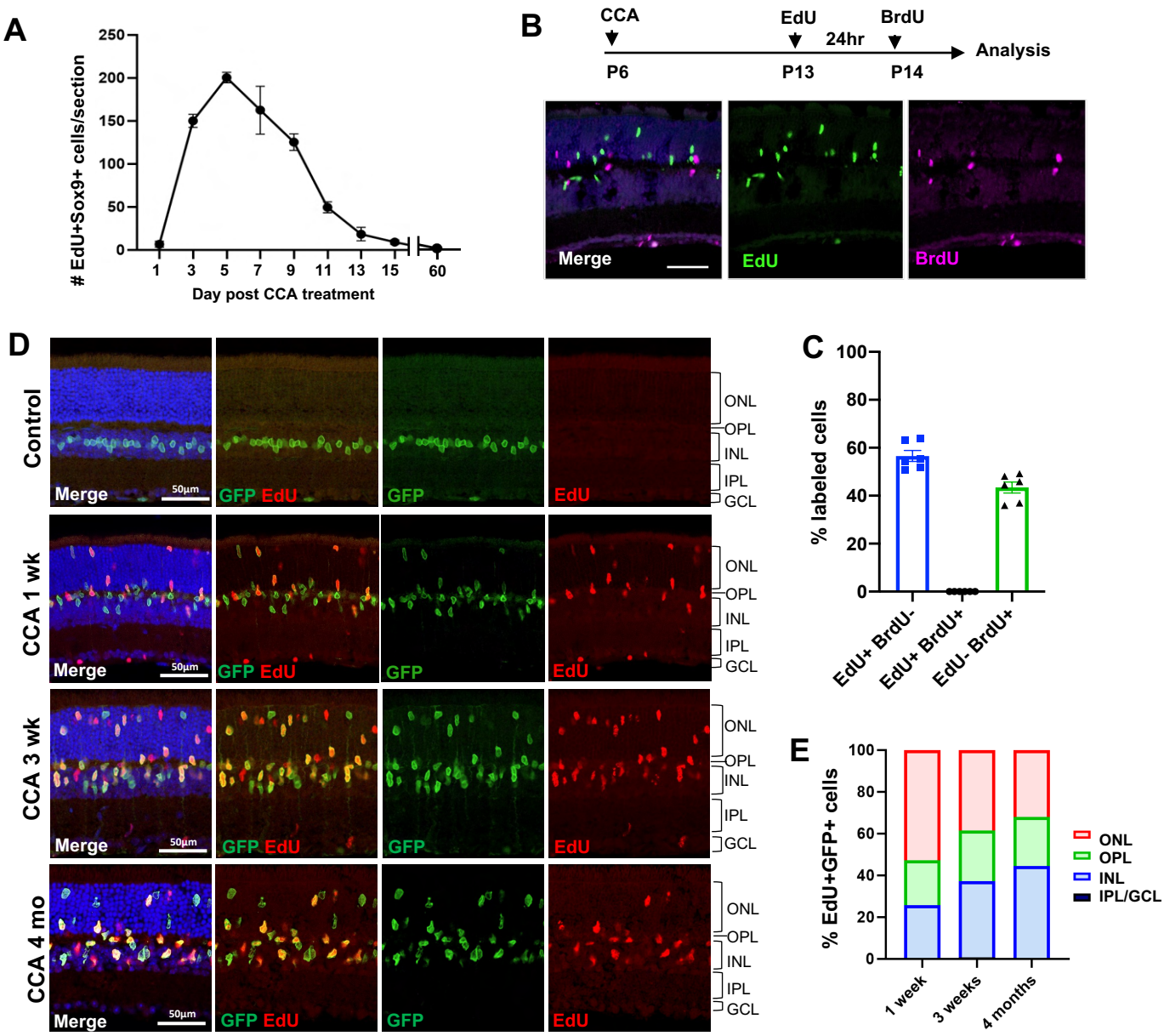
A
EdU+Sox9+ cells/section
250
200
150
100
50
0
1
3
5
7
9
11
13
15
60
Day post CCA treatment
B
CCA
EdU
BrdU
24hr
Analysis
P6
P13
P14
Merge
EdU
BrdU
D
Control
CCA 1 wk
CCA 3 wk
CCA 4 mo
Merge
50µm
GFP EdU
GFP
EdU
ONL
OPL
INL
IPL
GCL
C
% labeled cells
100
80
60
40
20
0
EdU+ BrdU-
EdU+ BrdU+
EdU- BrdU+
E
% EdU+GFP+ cells
1 week
3 weeks
4 months
ONL
OPL
INL
IPL/GCL

Figure 3

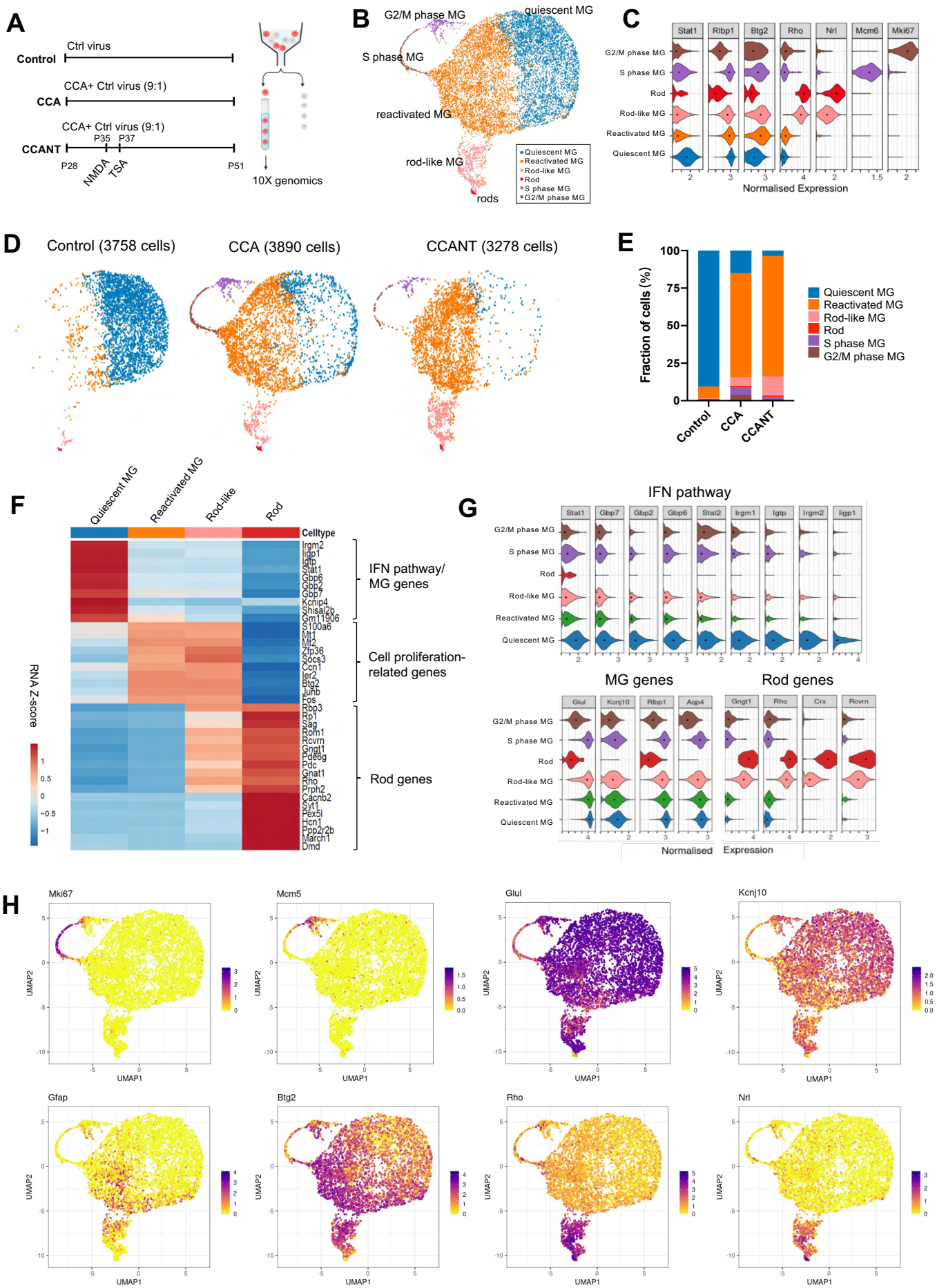
A
Control
Ctrl virus
CCA
CCA+ Ctrl virus (9:1)
CCANT
CCA+ Ctrl virus (9:1)
P35
P37
P28
P51
NMDA
TSA
10X genomics
B
G2/M phase MG
quiescent MG
S phase MG
reactivated MG
rod-like MG
rods
Quiescent MG
Reactivated MG
Rod-like MG
Rod
S phase MG
G2/M phase MG
C
Stat1
Rlbp1
Btg2
Rho
Nrl
Mcm6
Mki67
G2/M phase MG
S phase MG
Rod
Rod-like MG
Reactivated MG
Quiescent MG
Normalised Expression
D
Control (3758 cells)
CCA (3890 cells)
CCANT (3278 cells)
E
Fraction of cells (%)
100
75
50
25
0
Control
CCA
CCANT
Quiescent MG
Reactivated MG
Rod-like MG
Rod
S phase MG
G2/M phase MG
F
Quiescent MG
Reactivated MG
Rod-like
Rod
Celltype
Irgm2
Iigp1
Igtp
Stat1
Gbp6
Gbp2
Gbp7
Kchip4
Shisal2b
Gm11906
S100a6
Mt1
Mt2
Zfp36
Socs3
Ccn1
Ier2
Btg2
Junb
Fos
Rbp3
Rp1
Sag
Rom1
Rcvrn
Gngt1
Pde6g
Pdc
Gnat1
Rho
Prph2
Cacnb2
Syt1
Pex5l
Hcn1
Ppp2r2b
March1
Dmd
IFN pathway/
MG genes
Cell proliferation-
related genes
Rod genes
RNA Z-score
1
0.5
0
−0.5
−1
G
IFN pathway
Stat1
Gbp7
Gbp2
Gbp6
Stat2
Irgm1
Igtp
Irgm2
Iigp1
G2/M phase MG
S phase MG
Rod
Rod-like MG
Reactivated MG
Quiescent MG
MG genes
Rod genes
Glul
Kcnj10
Rlbp1
Aqp4
Gngt1
Rho
Crx
Rcvrn
Normalised Expression
H
Mki67
Mcm5
Glul
Kcnj10
Gfap
Btg2
Rho
Nrl
UMAP1
UMAP2

Figure 4

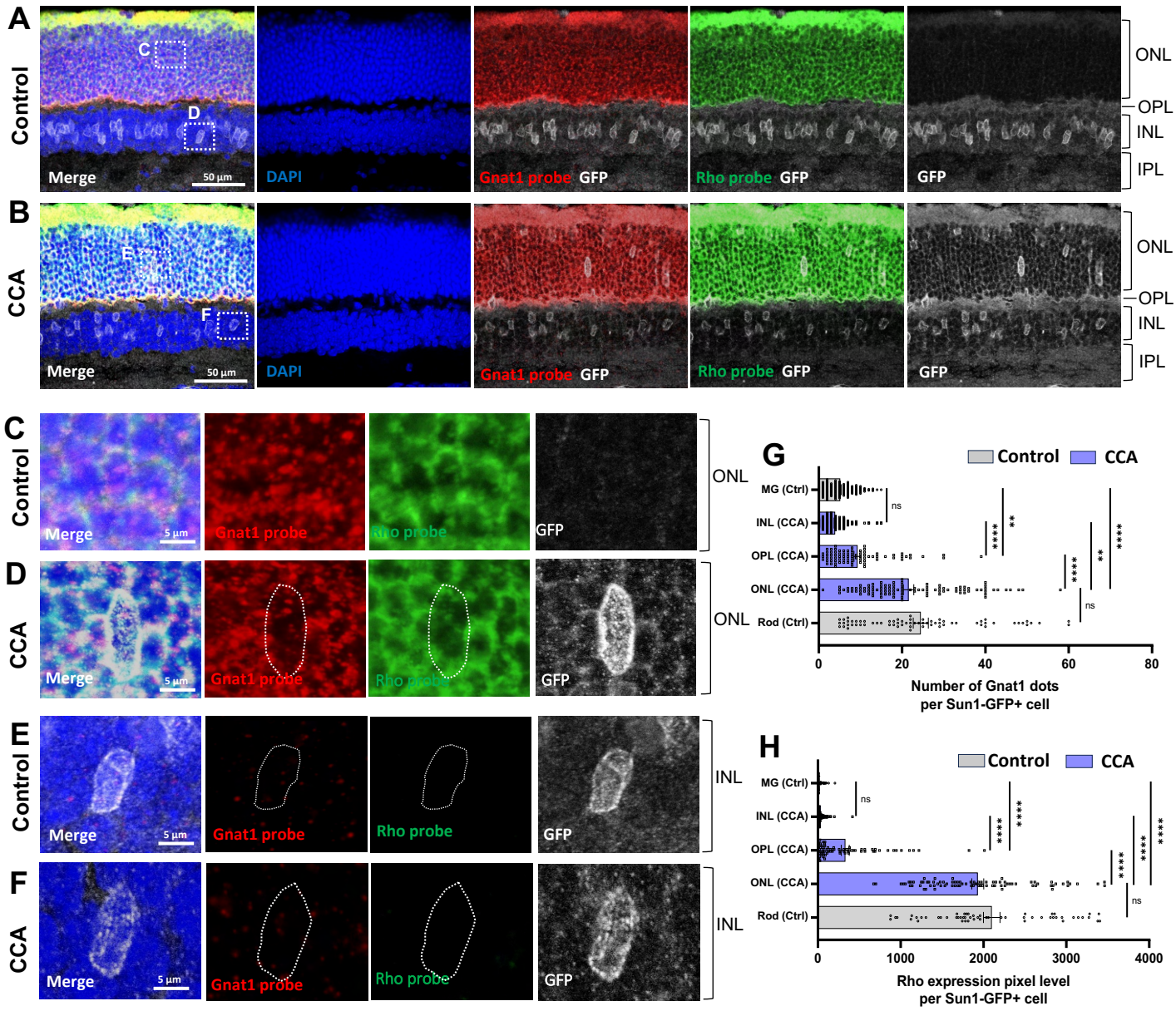
A
Control
C
D
Merge
50 µm
DAPI
Gnat1 probe GFP
Rho probe GFP
GFP
ONL
OPL
INL
IPL
B
CCA
E
F
Merge
50 µm
DAPI
Gnat1 probe GFP
Rho probe GFP
GFP
ONL
OPL
INL
IPL
C
Control
Merge
5 µm
Gnat1 probe
Rho probe
GFP
ONL
D
CCA
Merge
5 µm
Gnat1 probe
Rho probe
GFP
ONL
E
Control
Merge
5 µm
Gnat1 probe
Rho probe
GFP
INL
F
CCA
Merge
5 µm
Gnat1 probe
Rho probe
GFP
INL
G
Control
CCA
MG (Ctrl)
INL (CCA)
OPL (CCA)
ONL (CCA)
Rod (Ctrl)
ns
**
****
***
0
20
40
60
80
Number of Gnat1 dots
per Sun1-GFP+ cell
H
Control
CCA
MG (Ctrl)
INL (CCA)
OPL (CCA)
ONL (CCA)
Rod (Ctrl)
ns
****
***
0
1000
2000
3000
4000
Rho expression pixel level
per Sun1-GFP+ cell

Figure 5

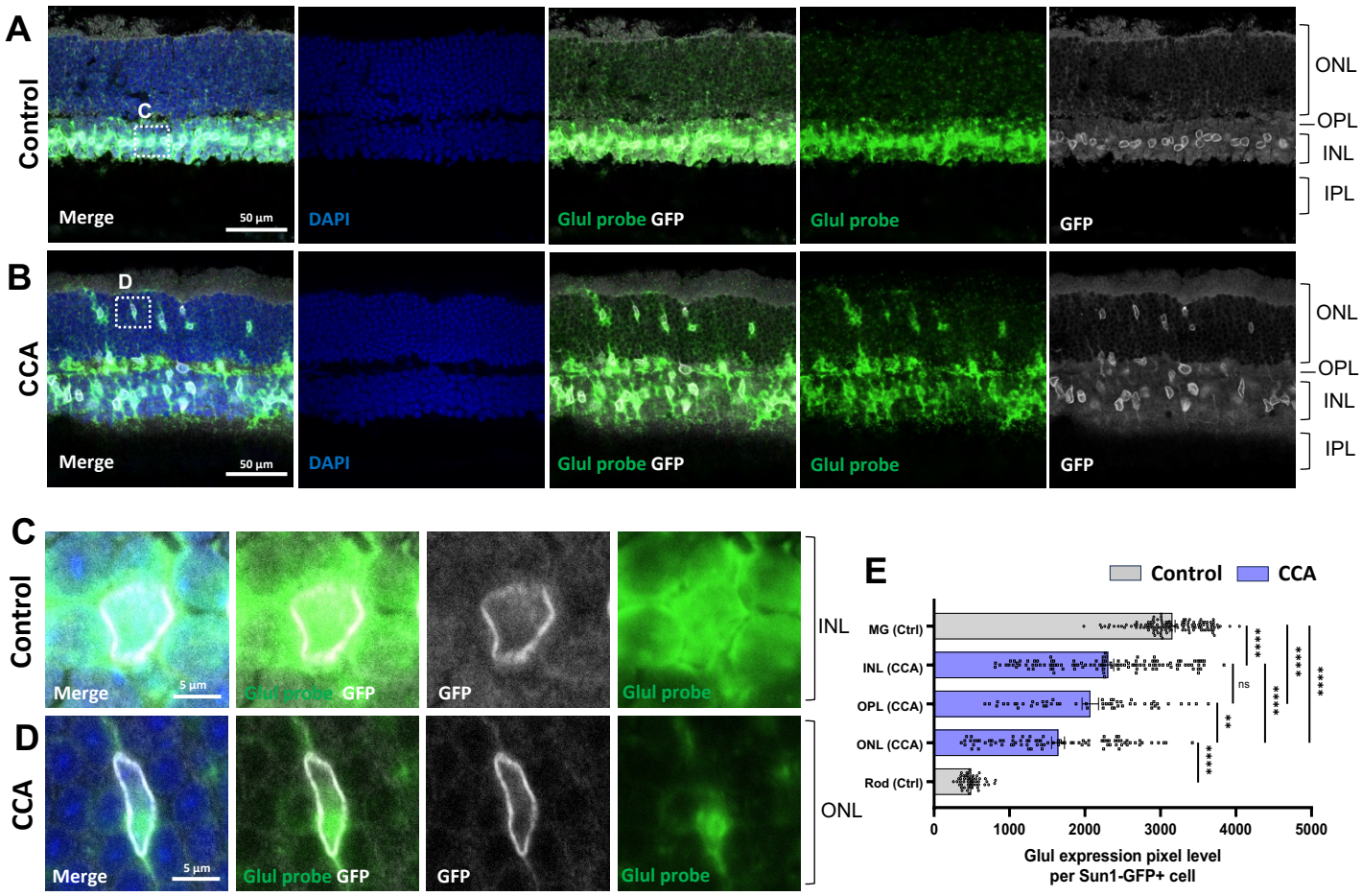
A
Control
C
Merge
50 µm
DAPI
Glul probe GFP
Glul probe
GFP
ONL
OPL
INL
IPL
B
CCA
D
Merge
50 µm
DAPI
Glul probe GFP
Glul probe
GFP
ONL
OPL
INL
IPL
C
Control
Merge
5 µm
Glul probe GFP
GFP
Glul probe
INL
D
CCA
Merge
5 µm
Glul probe GFP
GFP
Glul probe
ONL
E
Control
CCA
MG (Ctrl)
INL (CCA)
OPL (CCA)
ONL (CCA)
Rod (Ctrl)
ns
**
****
0
1000
2000
3000
4000
5000
Glul expression pixel level
per Sun1-GFP+ cell

Figure 6

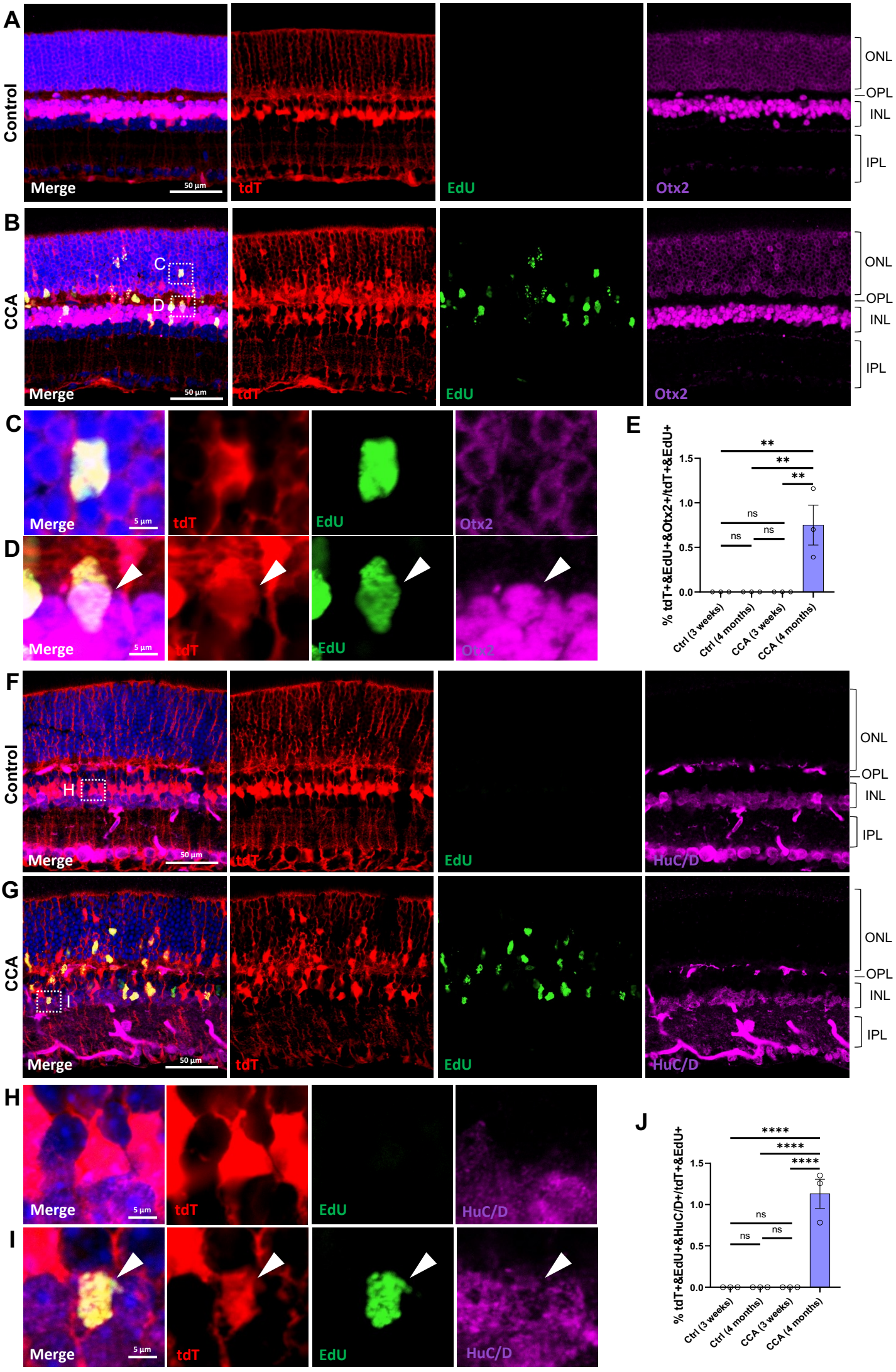
A
Control
Merge
50 µm
tdT
EdU
Otx2
ONL
OPL
INL
IPL
B
CCA
C
D
Merge
50 µm
tdT
EdU
Otx2
ONL
OPL
INL
IPL
C
Merge
5 µm
tdT
EdU
Otx2
D
Merge
5 µm
tdT
EdU
Otx2
E
% tdT+&EdU+&Otx2+/tdT+&EdU+
1.5
1.0
0.5
0.0
**
**
**
ns
ns
ns
Ctrl (3 weeks)
Ctrl (4 months)
CCA (3 weeks)
CCA (4 months)
F
Control
H
Merge
50 µm
tdT
EdU
HuC/D
ONL
OPL
INL
IPL
G
CCA
I
Merge
50 µm
tdT
EdU
HuC/D
ONL
OPL
INL
IPL
H
Merge
5 µm
tdT
EdU
HuC/D
I
Merge
5 µm
tdT
EdU
HuC/D
J
% tdT+&EdU+&HuC/D+/tdT+&EdU+
1.5
1.0
0.5
0.0
****
****
****
ns
ns
ns
Ctrl (3 weeks)
Ctrl (4 months)
CCA (3 weeks)
CCA (4 months)

Figure 7

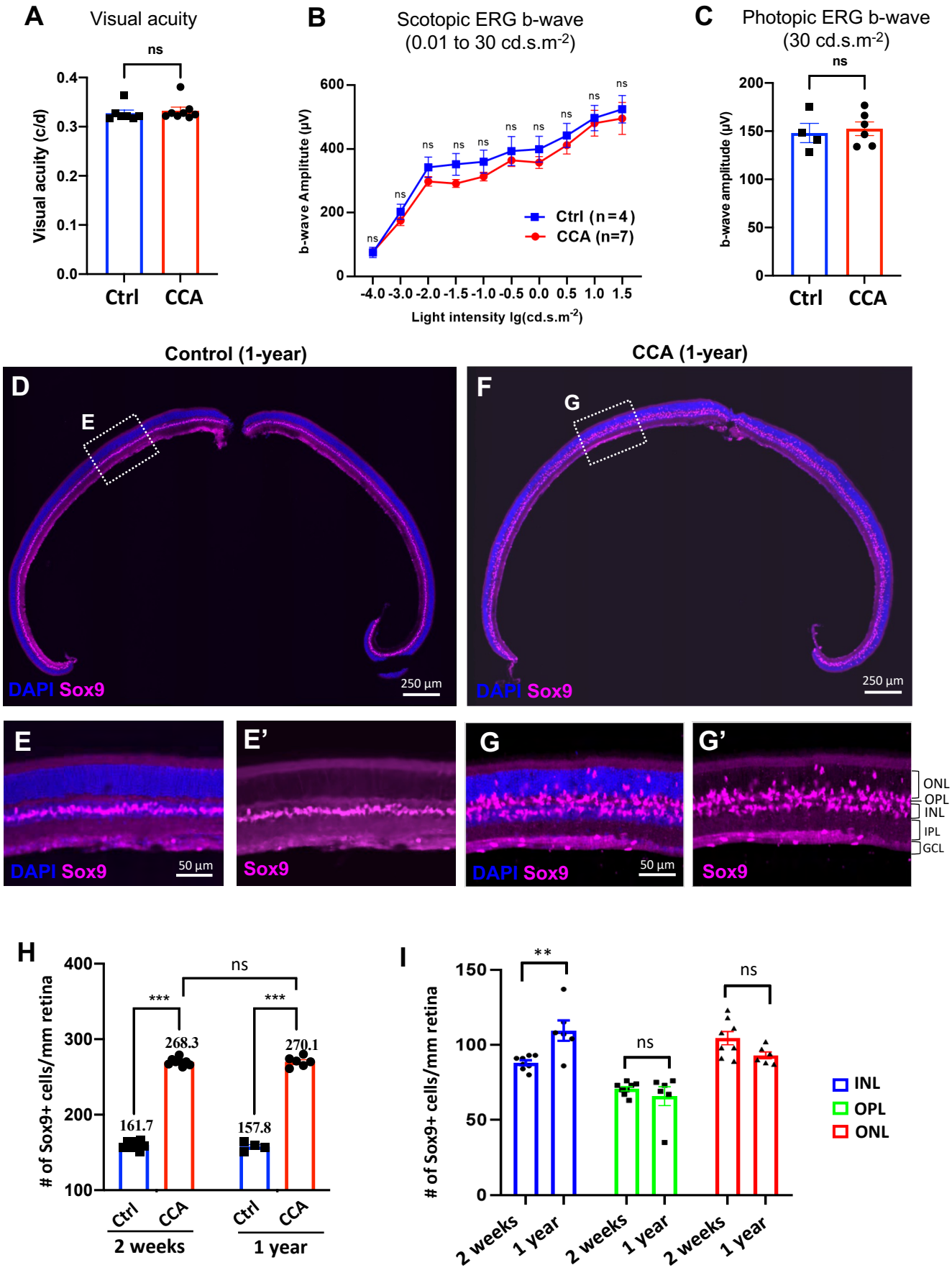
A
Visual acuity
ns
Visual acuity (c/d)
0.4
0.3
0.2
0.1
0.0
Ctrl
CCA
B
Scotopic ERG b-wave
(0.01 to 30 cd.s.m-2)
b-wave Amplitute (µV)
600
400
200
0
ns
Ctrl (n=4)
CCA (n=7)
-4.0 -3.0 -2.0 -1.5 -1.0 -0.5 0.0 0.5 1.0 1.5
Light intensity lg(cd.s.m-2)
C
Photopic ERG b-wave
(30 cd.s.m-2)
ns
b-wave amplitude (µV)
200
150
100
50
0
Ctrl
CCA
Control (1-year)
CCA (1-year)
D
E
F
G
DAPI Sox9
250 µm
E
E'
G
G'
DAPI Sox9
50 µm
Sox9
ONL
OPL
INL
IPL
GCL
H
# of Sox9+ cells/mm retina
400
300
200
100
***
ns
268.3
161.7
270.1
157.8
Ctrl
CCA
2 weeks
1 year
I
# of Sox9+ cells/mm retina
150
100
50
0
**
ns
2 weeks
1 year
INL
OPL
ONL